Unmasking Tandem Site Interaction in Human Acetylcholinesterase. Substrate Activation with a Cationic Acetanilide Substrate†

Joseph L. Johnson, Bernadette Cusack, Matthew P. Davies,‡ Abdul Fauq, and Terrone L. Rosenberry*

Departments of Pharmacology and Neurosciences, Mayo Foundation for Medical Education and Research, Mayo Clinic Jacksonville, Jacksonville, Florida 32224

Received October 25, 2002; Revised Manuscript Received January 16, 2003

ABSTRACT: Acetylcholinesterase (AChE) contains a narrow and deep active site gorge with two sites of ligand binding, an acylation site (or A-site) at the base of the gorge, and a peripheral site (or P-site) near the gorge entrance. The P-site contributes to catalytic efficiency by transiently binding substrates on their way to the acylation site, where a short-lived acyl enzyme intermediate is produced. A conformational interaction between the A- and P-sites has recently been found to modulate ligand affinities. We now demonstrate that this interaction is of functional importance by showing that the acetylation rate constant of a substrate bound to the A-site is increased by a factor a when a second molecule of substrate binds to the P-site. This demonstration became feasible through the introduction of a new acetanilide substrate analogue of acetylcholine, 3-(acetamido)-*N*,*N*,*N*-trimethylanilinium (ATMA), for which $a = 4$. This substrate has a low acetylation rate constant and equilibrates with the catalytic site, allowing a tractable algebraic solution to the rate equation for substrate hydrolysis. ATMA affinities for the A- and P-sites deduced from the kinetic analysis were confirmed by fluorescence titration with thioflavin T as a reporter ligand. Values of $a > 1$ give rise to a hydrolysis profile called substrate activation, and the AChE site-specific mutant W86F, and to a lesser extent wild-type human AChE itself, showed substrate activation with acetylthiocholine as the substrate. Substrate activation was incorporated into a previous catalytic scheme for AChE in which a bound P-site ligand can also block product dissociation from the A-site, and two additional features of the AChE catalytic pathway were revealed. First, the ability of a bound P-site ligand to increase the substrate acetylation rate constant varied with the structure of the ligand: thioflavin T accelerated ATMA acetylation by a factor a_2 of 1.3, while propidium failed to accelerate. Second, catalytic rate constants in the initial intermediate formed during acylation (*E*AP, where *E*A is the acyl enzyme and P is the alcohol leaving group cleaved from the ester substrate) may be constrained such that the leaving group P must dissociate before hydrolytic deacylation can occur.

Acetylcholinesterase (AChE)[1] catalyzes the hydrolysis of the neurotransmitter acetylcholine at one of the highest known enzymatic rates (*5*). Considerable progress has been made in understanding the mechanistic basis of this catalytic efficiency. Ligand binding studies (*7*) and X-ray crystallography (*8*) have revealed a narrow active site gorge some 20 Å deep with two separate ligand binding sites. At the base of the gorge is the acylation or A-site where residue W86[2] binds the trimethylammonium group of acetylcholine and H447, E334, and S203 participate in a triad that catalyzes the transient acylation and deacylation of S203 during each substrate turnover. The peripheral or P-site, spanned by residues W286 near the mouth of the gorge and D74 near a constriction at the boundary between the P-site and the A-site, specifically binds certain ligands such as the neurotoxin fasciculin (*9*−*12*) and the fluorescent probes propidium (*7*) and thioflavin T (*2*). Residues from Y74 through W86 comprise part of an ω-loop and extend along one side of the gorge from the P-site to the A-site.

In recent studies on human AChE we have begun to show how the P-site and the A-site work in tandem to optimize catalysis. The substrate acetylthiocholine [a chromogenic analogue of acetylcholine (Figure 1) with identical kinetic parameters] was found to bind to the P-site with a somewhat lower affinity than to the A-site (*6*), and this transient P-site binding contributes to catalytic efficiency by trapping substrates on their way to the A-site (*3*, *6*, *13*). The interaction of substrates with both the A- and the P-sites was not unexpected. Hydrolysis rates for cationic substrates have long

† This work was supported by Grant NS-16577 from the National Institutes of Health, by Grant DAMD 17-98-2-8019 from the U.S. Army Medical Research Acquisition Activity, by grants from the Muscular Dystrophy Association of America to T.L.R., and by NIH NRSA Fellowship NS-41828 to J.L.J.

* To whom correspondence should be addressed. Telephone: 904-953-7375. Fax: 904-953-7370. E-mail: rosenberry@mayo.edu.

‡ Current address: Department of Chemistry, University of California, Irvine, Irvine, CA 92697.

[1] Abbreviations: AChE, acetylcholinesterase; ATMA, 3-(acetamido)-*N*,*N*,*N*-trimethylanilinium; DEPQ, 7-[(diethoxyphosphoryl)oxy]-1-methylquinolinium iodide; DTNB, 5,5′-dithiobis(2-nitrobenzoic acid); NAP, 3-[1-(dimethylamino)ethyl]phenol; TMTFA, *m*-(*N*,*N*,*N*-trimethylammonio)trifluoroacetophenone.

[2] Throughout this paper we number amino acid residues according to the human AChE sequence.

10.1021/bi027065u CCC: $25.00
Published on Web 04/16/2003

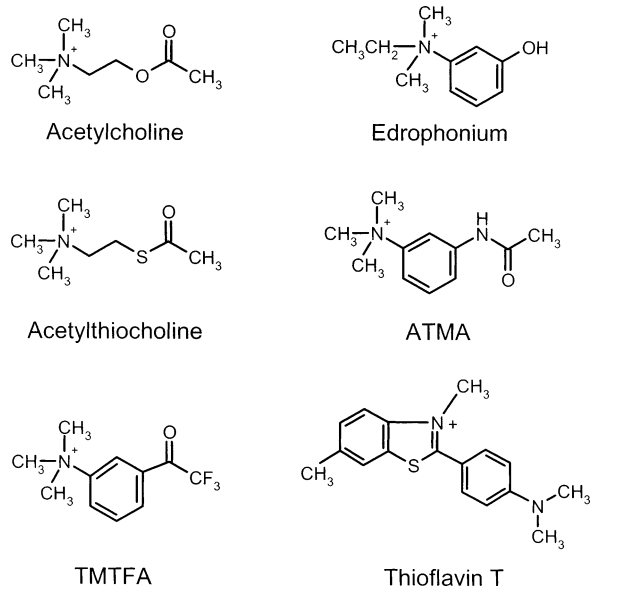

FIGURE 1: Structures of acetylcholine analogues and thioflavin T utilized in these studies.

been known to deviate from a classical Michaelis−Menten dependence on substrate concentration, with substrate inhibition seen at high substrate concentrations (*14*), and substrate inhibition was proposed to result from substrate binding to a peripheral site (*15*, *16*). Ligands that bind specifically to the P-site do inhibit substrate hydrolysis, and much of this inhibition results from a process that we have denoted steric blockade (*3*, *6*, *17*). Steric blockade is simply a reduction in association and dissociation rate constants for ligand binding to the A-site when a second ligand is already bound to the P-site. For example, substrate inhibition with acetylthiocholine arises from steric blockade of thiocholine product release from the A-site by a molecule of acetylthiocholine bound to the P-site (*3*, *6*). Steric blockade also is sufficient to account for the inhibition of substrate hydrolysis observed when small, reversible inhibitors bind specifically to the P-site (*2*, *6*, *17*).

The P-site is likely to play additional roles in AChE catalysis. One possibility is that ligand binding to the P-site alters reaction rate constants for substrates bound to the A-site. Changeux (*18*), who was among the first to appreciate that AChE contained two distinct ligand binding sites, suggested that allosteric interactions between ligands bound at these sites might involve conformational changes in the protein molecule. Solid evidence of ligand-induced conformational changes in AChE has recently been obtained from studies with fluorescent reporter groups (*2*, *19*). Furthermore, there may be functional consequences to conformational interaction between these sites. In a phenomenon called substrate activation, hydrolysis rates for cationic substrates again deviate from a classical Michaelis−Menten dependence on substrate concentration, but now with rates higher than predicted at moderate substrate concentrations. Such acceleration of the catalytic reaction cannot arise simply from ligand trapping and steric blockade at the P-site, effects that do not require conformational interaction between the P- and A-sites. Substrate activation was first observed in the cholinesterase gene family with horse serum butyrylcholinesterase (BChE) (*20*−*22*) but has not been apparent for wild-type AChE from mammals, electric eel, or *Torpedo*. Furthermore, BChE and, more strikingly, wild-type *Drosophila* AChE were characterized by triphasic substrate hydrolysis curves, with substrate activation at intermediate substrate concentrations and substrate inhibition at high substrate concentrations (*23*, *24*). In this paper, we briefly examine substrate activation with acetylthiocholine in wild-type human AChE and the W86F mutant and then introduce the new acetanilide substrate ATMA, whose structure (Figure 1) is very similar to that of acetylcholine and the transition state analogue TMTFA (*12*). This substrate shows triphasic hydrolysis curves with wild-type human AChE, and its slow turnover allows equilibrium analysis both of the hydrolysis kinetics and of fluorescence titrations in the presence of thioflavin T. The data are quantitatively consistent with a model in which substrate binding to the P-site gives rise to both substrate activation and substrate inhibition by acting on different steps in the catalytic pathway.

EXPERIMENTAL PROCEDURES

Materials. Recombinant human AChE was expressed as a secreted, disulfide-linked dimer in *Drosophila* S2 cells and purified as outlined previously (*25*). The W86F mutant of human AChE was constructed by procedures similar to those described previously for D74G AChE (*3*). The D74G and W86F AChEs were purified from culture medium by two cycles of affinity chromatography on acridinium resin (*1*). The affinity chromatography procedure was modified in that NaCl concentrations used during the washing steps did not exceed 100 mM and TX-100 was reduced to 0.02% to prevent excess stripping of bound protein off the column. Purified recombinant AChE samples analyzed by SDS−PAGE (*26*) showed no contaminants. Thioflavin T and *o*-nitrophenyl acetate were from Sigma. Thioflavin T was recrystallized from water, and concentrations were assigned by absorbance at 412 nm with $\epsilon_{412nm} = 36000\ M^{-1}\ cm^{-1}$. Concentrations of propidium iodide (Calbiochem) were determined with an extinction coefficient $\epsilon_{493nm} = 5900\ M^{-1}\ cm^{-1}$ (*7*). TMTFA (kindly provided by Dr. Daniel Quinn, University of Iowa) concentrations were calibrated by absorbance at 225 nm using $\epsilon_{225nm} = 43900\ M^{-1}\ cm^{-1}$.

Syntheses of 3-(Acetamido)-N,N,N-trimethylanilinium Iodide (ATMA) and 3-Amino-N,N,N-trimethylanilinium Iodide. A heterogeneous mixture of 3-amino-*N*,*N*-dimethylaniline dihydrochloride (Aldrich; 5.0 g, 24 mmol) and triethylamine (12.6 mL, 91 mmol) in 150 mL of dichloromethane was cannulated into a stirred solution of acetyl chloride (2.1 mL, 29 mmol) in dichloromethane cooled to −10 °C. The resulting mixture was left stirred for 2 h at 0 °C and for 12 h at room temperature. Water was added, and the dichloromethane solution was separated in a separatory funnel. After concentration and silica gel chromatography (using 50−60% ethyl acetate/hexane as eluent), *N*-[3-(dimethylamino)phenyl]acetamide (compound I) was isolated as a clear oil: yield 3.1 g (72%); ^{1}H NMR ($CDCl_3$) δ 7.25 (1H, br s, NH), 7.17 (1H, t, 1H, $J = 8.2$ Hz), 7.08 (1H, br s), 6.76 (1H, br d, $J = 7.8$ Hz), 6.52 (1H, br d, $J = 8.2$ Hz), 2.92 (6H, s), 2.12 (3H, s); IR (thin film) 1670 cm^{-1}.

A homogeneous mixture of compound I (300 mg, 1.7 mmol) and iodomethane (8 mL) was left standing in the dark at room temperature overnight. The white crystals produced were dissolved in hot water and treated with charcoal.

Cooling the aqueous filtrate gave pure ATMA in essentially quantitative yield: ^{1}H NMR (D_2O) δ 8.06 (1H, br m), 7.58−7.55 (2H, m), 7.51 (1H, m), 3.51 (9H, s), 2.12 (3H, s); IR (solid) 1679 cm^{-1}; MS [235, M^+ − (acetyl + methyl)].

3-Amino-*N*,*N*,*N*-trimethylanilinium chloride has been prepared from ATMA by refluxing in 50% (v/v) ethanol−concentrated HCl for 2 h (*27*). We employed an alternative procedure in which 3-amino-*N*,*N*-dimethylaniline dihydrochloride was converted to its butyloxycarbonate (BOC) derivative (dibutyl dicarbonate, dioxane, Na_2CO_3, H_2O) and then methylated in MeI as solvent to give *N*-BOC-*N*′,*N*′,*N*′-trimethylanilinium iodide. Removal of the BOC protecting group (dry HCl, ethyl acetate) followed by HPLC purification afforded pure 3-amino-*N*,*N*,*N*-trimethylanilinium chloride: ^{1}H NMR (D_2O) δ 7.21 (1H, br d, J = 7.72 Hz), 7.67 (2H, m), 7.42 (1H, br d, J = 8.6 Hz), 3.59 (9H, s).

Steady-State Measurements of AChE-Catalyzed Substrate Hydrolysis. Hydrolysis rates v were measured by spectrophotometry in 60 mM NaCl, 20 mM sodium phosphate, and 0.02% Triton X-100 at 25 °C. To maintain constant ionic strength when the concentrations of the cationic substrates acetylthiocholine and ATMA exceeded 1 mM, NaCl concentrations were decreased such that the sum of the substrate and NaCl concentrations was 60 mM. The pH was adjusted to 7.0 unless otherwise noted. Three substrates were employed. With acetylthiocholine, thiocholine generated in the presence of 0.33 mM DTNB (*28*) was determined by formation of the thiolate dianion of DTNB at 412 nm [$\Delta\epsilon_{412nm}$ = 14150 M^{-1} cm^{-1} at pH 7.3 (*29*)]. Hydrolysis of *o*-nitrophenyl acetate was measured by the appearance of *o*-nitrophenol (pK_a = 7.0) at its isosbestic point at 373 nm ($\Delta\epsilon_{373nm}$ = 2800 M^{-1} cm^{-1}). With ATMA, the formation of the aniline hydrolysis product 3-amino-*N*,*N*,*N*-trimethylanilinium (pK_a = 2.4) was followed at 290 nm ($\Delta\epsilon_{290nm}$ = 1850 M^{-1} cm^{-1}) for ATMA concentrations below 5 mM and at 310 nm ($\Delta\epsilon_{310nm}$ = 465 M^{-1} cm^{-1}) for higher concentrations. Concentrations of the substrate stocks were established by absorbance measurements following complete AChE-catalyzed hydrolysis to their respective products: thiocholine as the thiolate dianion of DTNB at 412 nm [$\epsilon_{412nm} \cong \Delta\epsilon_{412nm}$ = 14150 M^{-1} cm^{-1} (*29*)]; *o*-nitrophenol (λ_{max} at 416 nm, ϵ_{416nm} = 5600 M^{-1} cm^{-1} in 0.1 N NaOH; λ at 373 nm, ϵ_{373nm} = 3000 M^{-1} cm^{-1}); and 3-amino-*N*,*N*,*N*-trimethylanilinium (λ_{max} at 286 nm, ϵ_{286nm} = 1960 M^{-1} cm^{-1} at neutral pH). Reactions were recorded for 1−7 min on a Varian Cary 3A spectrophotometer. Substrate concentrations were corrected for substrate depletion resulting from hydrolysis during the assay, and hydrolysis rates v at the average assay interval t_{av} were adjusted for nonenzymatic hydrolysis. At very low substrate concentrations values of v were sometimes confirmed by fitting the complete time course of the absorbance A to the relationship $A = A_0 + \Delta A(1 - e^{-kt})$, where ΔA was fixed as the product of the initial substrate concentration and the difference extinction coefficient, and v at t_{av} was calculated as $v = \Delta A k e^{-kt_{av}}$. The ratio of monobasic and dibasic sodium phosphate (each 20 mM) was adjusted to obtain hydrolysis rates at pH 5.5. At pH 5.0, mixtures of 20 mM acetic acid and 20 mM sodium acetate were used in place of sodium phosphate to increase buffering. In these buffers, the value of $\Delta\epsilon_{412nm}$ for the thiolate dianion of DTNB was calculated on the basis of a pK_a of 4.53 (*29*), and the pH was confirmed at the end of each reaction. To stabilize AChE at pH 5.0 and 5.5, bovine serum albumin was added to each reaction to a final concentration of 0.1 wt %.

The total concentration of enzyme active sites ($[E]_{tot}$) for wild-type and D74G AChE was calculated by assuming 450 units/nmol (*2*, *3*).[3] For W86F AChE, $[E]_{tot}$ was determined by titrations with TMTFA (*17*) and DEPQ (*25*), and a calibration factor of 3.0 ΔA_{412nm}/min was established for 1 nM W86F AChE and 5 mM acetylthiocholine in 20 mM sodium phosphate and 0.02% Triton X-100 (pH 7.0) at 25 °C.

The second-order rate constant for substrate hydrolysis was denoted k_{cat}/K_{app}. As the substrate concentration [S] approaches zero, $v/[E]_{tot} = (k_{cat}/K_{app})[S]$ for virtually all models of AChE hydrolysis. Before hydrolysis rates for a full range of substrate concentrations were fitted to models below, k_{cat}/K_{app} was determined by applying the Michaelis−Menten expression $v/[E]_{tot} = (k_{cat}/K_{app})[S]/(1 + [S]/K_{app})$ over the range $[S] < 0.6K_{app}$. When data sets with slightly different k_{cat}/K_{app} determinations were combined on one graph with a mean $(k_{cat}/K_{app})_M$, $[E]_{tot}$ was normalized to $[E]_N$ such that $(k_{cat}/K_{app})_M[E]_N = (k_{cat}/K_{app})[E]_{tot}$.

A Two-Site Model of ATMA Hydrolysis. Schemes 4 and 5 (Appendix) and eq 5 (Appendix) present mechanistic models for substrate inhibition and substrate activation. For efficient substrates such as acetylthiocholine, quantitative examination of these models is challenging. However, with substrates for which k_2 in Scheme 5 is sufficiently small, all reversible reactions reach equilibrium, and solution of the steady-state rate equations is simplified considerably. To decrease k_2 into this range, we introduced the cationic acetanilide substrate ATMA. The ratio of k_2 to k_3 for this substrate with AChE is about 10^3-fold lower than that for acetylthiocholine. The low value of k_2 not only allows the equilibrium assumptions but also reduces the acetyl enzyme *E*A and all its ligand complexes in Scheme 5 to negligible levels. Scheme 5 then is condensed to Scheme 1.

Scheme 1

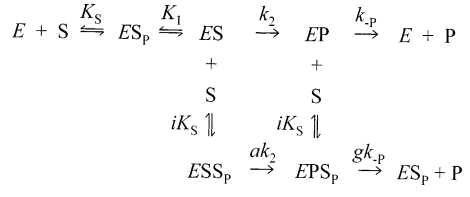

In this scheme as in Scheme 5, the acylation rate constant k_2 is altered by the factor a in the ESS_P ternary complex, and the dissociation rate constant k_{-P} of the product (here 3-amino-*N*,*N*,*N*-trimethylanilinium) is altered by the factor g when substrate is bound to the P-site prior to product dissociation. The equilibrium dissociation constants $K_S = k_{-S}/k_S$ and $K_1 = k_{-1}/k_1$. The steady-state equations for Scheme 1 may be solved algebraically to give eq 1. In eq 1, $K_M = K_S K_1$. The second-order rate constant $k_{cat}/K_{app} \equiv k_2/K_M$ was measured as noted above at low substrate concentration, and the full eq 1 was then fitted with three

[3] One unit of AChE activity corresponds to 1 μmol of acetylthiocholine hydrolyzed/min under standard pH-stat assay conditions at pH 8 (*1*, *2*). Our conventional spectrophotometric assay at 412 nm is conducted in pH 7 buffer. With wild-type AChE and 0.5 mM acetylthiocholine, this assay results in 4.8 ΔA_{412nm}/min with 1 nM AChE or about 76% of the pH-stat assay standard.

fixed parameters (k_2/K_M, i, and g) and four variables (iK_S, K_M, a, and k_{-P}).

$$\frac{v}{[E]_{tot}} = \frac{k_2 \frac{[S]}{K_M}\left(1+\frac{a[S]}{iK_S}\right)}{1+\frac{i[S]}{iK_S}+\frac{[S]}{K_M}\left(1+\frac{[S]}{iK_S}\right)\left[1+\frac{k_2}{k_{-P}}\frac{\left(1+\frac{a[S]}{iK_S}\right)}{\left(1+\frac{g[S]}{iK_S}\right)}\right]} \quad (1)$$

Inclusion of a P-site inhibitor during hydrolysis of ATMA results in the extension of Scheme 1 to Scheme 6 and eq 1 to eq 6 as presented in the Appendix.

Inhibition Constants for Reversible Inhibitors. At low concentrations of all the substrates used in this study, reciprocal plots of v^{-1} vs $[S]^{-1}$ were linear in the absence and the presence of a fixed concentration of an inhibitor I. Slopes of these plots were calculated by weighted linear regression analyses assuming that v has a constant percent error. These slopes were reciprocals of the apparent second-order hydrolysis rate constants z. In the absence of I, z is denoted $z_{I=0} = V_{max}/K_{app}$. Measured z at various [I] were fitted according to eq 2 by weighted nonlinear regression analyses

$$\frac{z_{I=0}}{z} = \frac{1+[I]/K_I}{1+\alpha[I]/K_I} \quad (2)$$

to obtain the inhibition constant K_I and the experimental parameter α (*2*, *17*).[4] K_I is the equilibrium dissociation constant for I with E. The constant α is simply the ratio of the second-order rate constant with saturating I to that in the absence of I.

Determination of Ligand Affinities for the P-Site by Fluorescence Titration with Thioflavin T. The fluorescence of thioflavin T is enhanced when bound to the AChE P-site (*2*). Fluorescence was monitored on either a Perkin-Elmer LS-50B luminescence spectrometer or a Cary Eclipse fluorescence spectrophotometer. The sample for each experimental point was premixed and then measured in 0.2−2 mL cuvettes at pH 7.0 in 60 mM NaCl, 20 mM sodium phosphate, and 0.02% Triton X-100 with thermostating at 23 °C. To maintain constant ionic strength when the concentration of ATMA exceeded 1 mM, NaCl concentrations were decreased such that the sum of the ATMA and NaCl concentrations was 60 mM. Thioflavin T fluorescence (F) was measured with excitation at 450 nm and emission either fixed at 490 nm or scanned from 480 to 530 nm with excitation and emission slits of 10−20 nm. When scans were obtained, total areas under the fluorescence emission curves were calculated.

To restrict the fluorescence titrations to just the P-site and to minimize the effect of ATMA hydrolysis on the titrations, the A-site of AChE was blocked by inactivation with TMTFA or echothiophate. The inactivated enzymes were generated by incubating a 3-fold molar excess of TMTFA or echothiophate with 10−20 μM AChE for several hours at room temperature prior to dilution for fluorescence measurements. Residual enzyme activity was confirmed to be <0.03% of the initial activity by the standard acetylthiocholine assay.

In experiments with thioflavin T and AChE alone, measurements of F were analyzed with eq 3 (*2*, *30*). In eq

$$F = F_B + 0.5(f_{EL} - f_L)\left[D - \sqrt{D^2 - 4[E]_{tot}[L]_{tot}}\right] \quad (3)$$

3, $D = [E]_{tot} + [L]_{tot} + K_L$, where $[E]_{tot}$ and $[L]_{tot}$ are the total enzyme and thioflavin T concentrations, respectively, and K_L is the equilibrium dissociation constant; $F_B = B + f_L[L]_{tot} + f_E[E]_{tot}$, where B is the blank fluorescence without E or L; and f_L, f_{EL}, and f_E are the fluorescence intensity coefficients for free thioflavin T, bound thioflavin T, and free enzyme, respectively. Values of f_L and f_E were determined from measurements with thioflavin T or enzyme alone. Because the absorbance of thioflavin T was significant at the excitation wavelength ($\epsilon_{450nm} = 8500\ M^{-1}\ cm^{-1}$), observed F values (F_{obs}) were corrected (F_{corr}) for inner filter effects (*31*) as follows: $\log(F_{corr}) = \log(F_{obs}) + 0.5(A_{450})(path)$, where A_{450} is the absorbance at 450 nm and *path* is the path length of the excitation beam in the fluorescence cuvette. Data were fitted to eq 3 by nonlinear regression analysis (Fig.P), with either $[L]_{tot}$ or $[E]_{tot}$ as the independent variable. Initial fitting involved K_L, f_{EL}, and B as the fitted parameters, and values of F were weighted by assuming constant percent error. The fitted value of B was then fixed in an unweighted final fitting with K_L and f_{EL} as the fitted parameters.

In other experiments, thioflavin T fluorescence was employed to evaluate interactions of ATMA (S) at the A- and P-sites. Scheme 6 (Appendix) was simplified to Scheme 2 because intermediates involving EP were assumed negligible.

Scheme 2

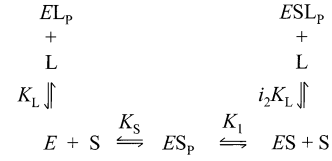

In this scheme the affinity of thioflavin T (L) at the P-site (denoted by subscript P) of AChE is characterized by the dissociation constant K_L in the absence of substrate and by i_2K_L when S occupies the acylation site. All reactions were assumed to reach equilibrium, and the fluorescence data were analyzed with eq 4. In eq 4, $F_B = B + f_L[L]_{tot} + f_S[S]_{tot}$,

$$F = F_B + \frac{[E]_{tot} f_{EL}\frac{[L]}{K_L}\left[1+\left(\frac{f_{ELS}}{f_{EL}}\right)\left(\frac{[S]}{i_2K_M}\right)\right]}{1+\frac{i[S]}{iK_S}+\frac{[L]}{K_L}+\frac{[S]}{K_M}\left[1+\frac{[S]}{iK_S}+\frac{[L]}{i_2K_L}\right]} \quad (4)$$

where B is the blank fluorescence with E in the absence of L or S. Values of f_L and f_S were determined from measurements with thioflavin T or ATMA alone. Data were fitted to eq 4 by nonlinear regression analysis (Fig.P), with [S] as the independent variable and values of F weighted by assuming constant percent error. With wild-type AChE, K_L, i, and i_2 were fixed, and K_M, iK_S, f_{EL}, and f_{EL}/f_{ELS} were the fitted parameters. With echothiophate- and TMTFA-inacti-

[4] This equation was inverted and thus incorrect in ref *6*.

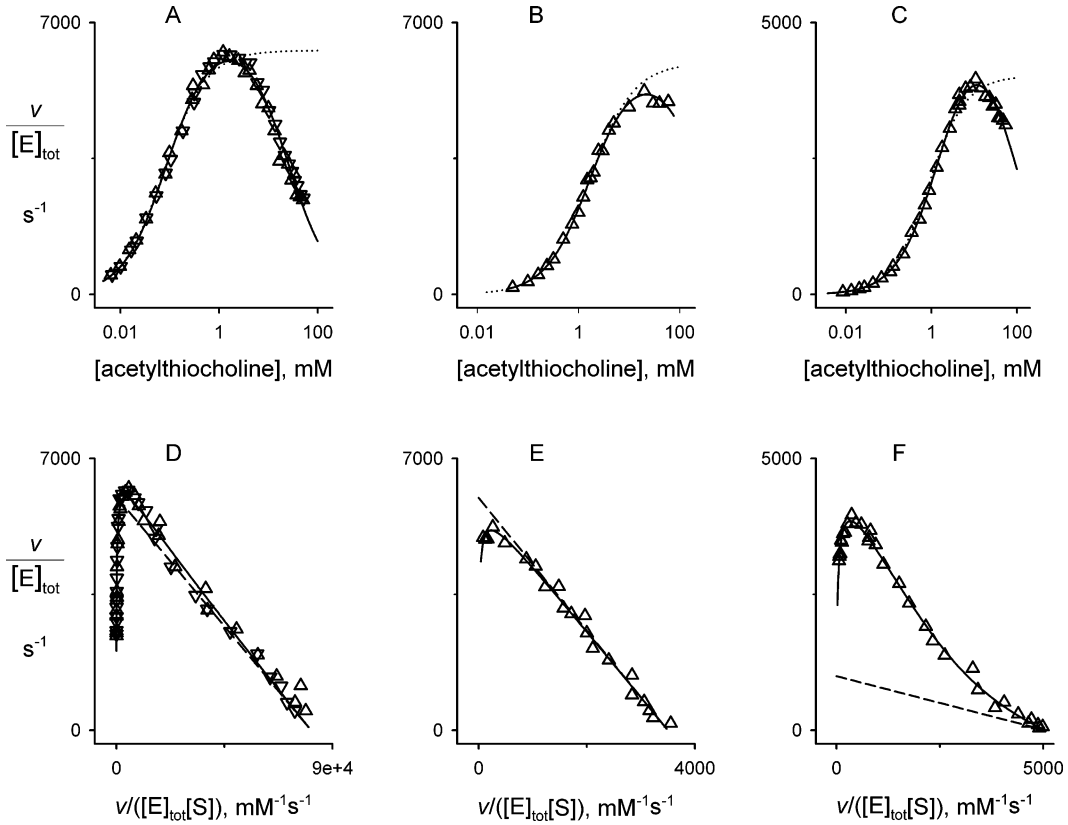

FIGURE 2: Substrate activation during acetylthiocholine hydrolysis is easily detected with human W86F AChE but not with wild-type or D74G AChE. Panels A−C: Representative plots of $v/[E]_{tot}$ vs [S] for wild type (A), D74G (B), and W86F (C) at pH 7.0. $[E]_{tot}$ corresponded to 80−150 pM in each case. The solid lines indicate analyses with eq 5 (as outlined in the Appendix) and predetermined fixed values of k_{cat}/K_{app} (Table 1) to give fitted parameters that are included in the averages in Table 1. Two independent data sets (△, ▽) were fitted simultaneously for the wild-type enzyme. The dotted lines correspond to the best fits of data below 5 mM [S] to the Michealis−Menten equation. Panels D−F: Data and fitted lines in panels A−C were transformed to the Eadie−Hofstee format (corresponding to $v/[E]_{tot}$ vs $v/[E]_{tot}[S]$) to clarify the substrate activation phase, which is indicated by the deviation of points above the dashed line calculated as outlined under eq 5 in the Appendix.

vated AChE, K_M^{-1} was set to zero, K_L was fixed, and K_S and f_{EL} were the fitted parameters.

RESULTS

Substrate Activation during Acetylthiocholine Hydrolysis Is Readily Observed with Human W86F AChE but Not with Wild-Type or D74G AChE. Substrate inhibition and substrate activation are defined as deviations from classical Michaelis−Menten substrate hydrolysis profiles. Profiles of acetylthiocholine hydrolysis by wild-type, D74G, and W86F AChEs are shown in Figure 2. In plots of normalized hydrolysis rates $v/[E]_{tot}$ vs the substrate concentration [S] in Figures 2A−C, substrate inhibition is recognized as a decrease from the maximum $v/[E]_{tot}$ at high [S]. It is more apparent with wild-type AChE in panel A and W86F AChE in panel C than with D74G AChE in panel B. D74 contributes to ligand affinity at the P-site (the acetylthiocholine affinity decreased 10−20-fold in D74G AChE), and this decrease in P-site affinity was sufficient to account for the nearly complete loss of substrate inhibition with D74G AChE (*3*). Substrate activation is defined as an increase in $v/[E]_{tot}$ from that corresponding to a hyperbolic Michaelis−Menten profile. Such a deviation is difficult to see in panels A−C of Figure 2, but it can become more evident when the *x*-axis is replotted in the Eadie−Hofstee format in Figure 2D−F. In this format, adherence to the Michaelis−Menten formulation results in a straight line of negative slope. The data for wild-type and D74G AChEs in Figure 2D,E conform to such linear plots until substrate inhibition intervenes at the left of each curve. However, data points for W86F AChE in Figure 2F at intermediate substrate concentrations fall above the dashed line established at low substrate concentrations before substrate inhibition again intervenes at the highest substrate concentrations. Therefore, W86F AChE shows substrate activation at intermediate concentrations as well as substrate inhibition at high concentrations.

Substrate inhibition and activation are important phenomena because they can reveal underlying features of an enzyme catalytic site. Unfortunately, quite different catalytic mechanisms can result in identical substrate hydrolysis profiles, and additional experimental data are necessary to select the appropriate mechanism. It is generally conceded that substrate inhibition or activation occurs only when a second molecule of substrate interacts with an enzyme catalytic intermediate produced by an initial substrate molecule. The resulting ternary complex can be as simple as *E*SS. Substrate inhibition occurs if *E*SS is unreactive, as proposed by Haldane (*32*). Alternatively, substrate activation arises if *E*SS undergoes catalytic turnover more rapidly than *E*S. Simple models limited to *E*SS are often invoked to allow fitting of substrate inhibition or substrate activation data with cholinesterases (e.g., refs *19* and *33*). However, these models are insufficient if a hydrolysis profile is triphasic, showing both substrate inhibition and activation, as in Figure 2F.

Table 1: Analysis of Substrate Hydrolysis According to the Three-Site Model in Scheme 4[a]

enzyme	substrate	pH	*n*	k_{cat}/K_{app} (mM^{-1} s^{-1})	a_{sa}	K_{sa} (mM)	K_{si} (mM)	K_d (mM)
W86F AChE	acetylthiocholine	7.0	5	5.0×10^3	5.8 ± 1.0	1.9 ± 0.2	86 ± 4	0.21 ± 0.06
D74G AChE[b]	acetylthiocholine	7.0	1	3.5×10^3	—[c]	—[c]	290 ± 60	1.71 ± 0.03
wild-type AChE	acetylthiocholine	7.0	11	7.7×10^4	1.15 ± 0.03	0.5 ± 0.2	26 ± 1	0.073 ± 0.007
wild-type AChE	acetylthiocholine	5.5	2	1.0×10^4	1.31 ± 0.08	4 ± 3	230 ± 90	0.127 ± 0.003
wild-type AChE	acetylthiocholine	5.0	1	2.5×10^3	2.0 ± 0.3	1.1 ± 0.3	700 ± 300	0.24 ± 0.04
wild-type AChE	ATMA	7.0	6	1.1×10^2	4.1 ± 0.2	2.7 ± 0.4	108 ± 8	0.045 ± 0.005

[a] Acetylthiocholine hydrolysis profiles (*n* independent sets) like those in Figures 2 and 3 were fitted with eq 5 to obtain the three equilibrium constants K_{sa}, K_{si}, and K_d and the relative acceleration constant a_{sa} in Scheme 4. ATMA hydrolysis profiles such as those in Figure 4 also were analyzed with eq 5. Values of k_{cat}/K_{app} employed in the analyses were obtained prior to fitting as outlined in the Experimental Procedures, and the average values are shown. In this and other tables in this report, listed values when $n > 1$ are unweighted means with standard errors of the mean; when $n = 1$, they are the fitted value with the standard error calculated from the fitting procedure. [b] Data for D74G was taken from ref *3*. [c] The fitted K_{sa}^{-1} was zero, removing a_{sa} as a variable.

Triphasic profiles also have been observed with *Drosophila* AChE, and a curve-fitting model involving substrate binding in two distinct ternary complexes was proposed (*34*). One ternary complex was unreactive and resulted in substrate inhibition, and the other complex resulted in acceleration of the catalytic pathway and substrate activation. We consider a similar curve-fitting model in Scheme 4 (Appendix), where substrate can bind to three enzyme sites. This model is very simple because it assumes equilibrium substrate binding and no interaction between sites. Its major advantage is that the corresponding rate equations can be solved algebraically (eq 5), providing kinetic parameters to quantify and compare triphasic profiles. For example, parameters for the W86F profile in Figure 2F (listed in Table 1) include the equilibrium dissociation constants for substrate binding to the activation site ($K_{sa} = 1.9$ mM), to the inhibition site ($K_{si} = 86$ mM), and to the catalytic site ($K_d = 0.21$ mM). Acetylthiocholine turnover in the ESS_{sa} complex is increased by the factor $a_{sa} = 5.8$ relative to turnover in the *E*S complex.

The three-site model detects a small substrate activation component with high sensitivity. Activation is indicated by an a_{sa} value greater than 1. Fitting of the hydrolysis profile for wild-type AChE in Figure 2A to eq 5 yielded $a_{sa} = 1.1 \pm 0.2$. Since this value is not significantly different from 1, it would be hard to conclude from this single profile that wild-type AChE shows substrate activation at pH 7.0. However, an average value of $a_{sa} = 1.15 \pm 0.03$ was obtained when a large number of profiles for wild-type AChE was analyzed (Table 1),[5] suggesting that a small but significant substrate activation does occur with wild-type AChE. Masson et al. recently reported that substrate activation with wild-type AChE is enhanced at lower pH (*35*), and we have confirmed this observation by analysis with eq 5 (Figure 3). At both pH 5.5 and pH 5.0, the points in Eadie−Hofstee plots fall above the dashed line in Figure 3B, and fitted values of a_{sa} were 1.31 and 1.97 at pH 5.5 and 5.0, respectively (Table 1). Therefore, wild-type human AChE at lower pH also shows triphasic substrate activation and substrate inhibition curves, although these effects are less pronounced than for the W86F mutant.

While Scheme 4 and eq 5 are useful for curve fitting and for detecting substrate inhibition and activation, they are of little help in understanding the AChE catalytic mechanism.

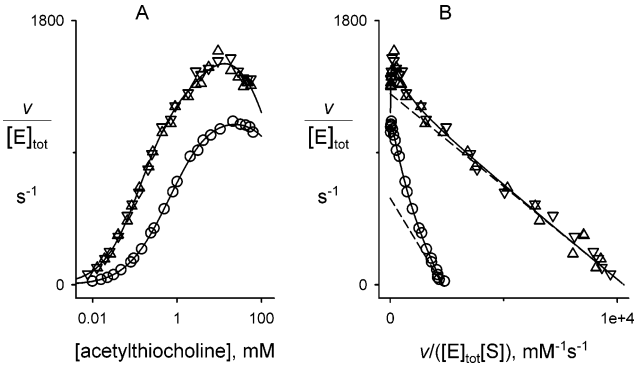

FIGURE 3: Substrate activation during acetylthiocholine hydrolysis by human wild-type AChE becomes more apparent at pH values below 7.0. Panel A: Plots of $v/[E]_{tot}$ vs [S] at pH 5.0 (○) and for two independent data sets at pH 5.5 (△, ▽). $[E]_{tot}$ corresponded to 300−800 pM. The solid lines were fitted with eq 5 to obtain the parameters indicated in Table 1. Panel B: Data and fitted lines in panel A were transformed to the Eadie−Hofstee format to clarify the substrate activation phase as in Figure 2.

As noted in the introduction, the A- and P-sites in the AChE catalytic site are well established, but there is no evidence for the third independent substrate binding site postulated in Scheme 4. It thus becomes a mechanistic challenge to account for triphasic hydrolysis profiles such as that for W86F in Figure 2 with a model involving only the A- and P-sites. Scheme 5 (Appendix) proposes such a model. This scheme, which we proposed previously (*3*, *6*), makes explicit four A-site intermediates on the catalytic pathway and allows consideration of the effects of substrate binding to the P-site on each of them. If the binding of substrate (S) had no effect ($a = b = g = i = 1$ in Scheme 5), hydrolysis data such as that in Figure 2 would follow Michaelis−Menten profiles. To account for hydrolysis data for acetylthiocholine and wild-type AChE, where substrate inhibition is the predominant deviation from a Michaelis−Menten profile (Figure 2A), it was sufficient to restrict effects to just one reaction, product dissociation from intermediates $EAPS_P$ and EPS_P, as proposed in our steric blockade model (*3*, *6*, *17*). Hydrolysis data were fitted to this model with the SCoP program outlined in the Appendix. When the rate constant k_{-P} for product dissociation was reduced by the factor *g* with S bound to the P-site, substrate inhibition data with wild-type AChE like that in Figure 2A were accurately fitted with *g* values approaching 0.01 (*3*, *6*, *17*). We now find that, if this steric blockade assumption ($g = 0.01$) is retained and the relative acetylation rate constant *a* or deacetylation rate

[5] A large number of hydrolysis profiles for wild-type AChE were generated in analyzing inhibition patterns by various inhibitors for a manuscript in preparation.

Table 2: Analysis of Substrate Hydrolysis According to the Two-Site Model in Schemes 5 and 1[a]

enzyme	substrate	pH	*n*	*a*	iK_s (mM)	k_{-P} (s^{-1})	k_2 (s^{-1})	K_M (mM)
W86F AChE	acetylthiocholine	7.0	5	16 ± 7	2.3 ± 0.3	$(1.2 \pm 0.1) \times 10^5$	$(9 \pm 3) \times 10^2$	
wild-type AChE	acetylthiocholine	7.0	11	1.9 ± 0.2	0.9 ± 0.2	$(1.2 \pm 0.1) \times 10^5$	$(1.2 \pm 0.02) \times 10^4$	
wild-type AChE	acetylthiocholine	5.5	2	7 ± 1	3.3 ± 0.2	$(5.3 \pm 0.3) \times 10^4$	$(1.8 \pm 0.2) \times 10^3$	
wild-type AChE	acetylthiocholine	5.0	1	4	3	7×10^4	1.5×10^3	
wild-type AChE	ATMA	7.0	6	4.1 ± 0.2	2.7 ± 0.4	700 ± 100	5.3 ± 0.4	0.047 ± 0.006

[a] The acetylthiocholine hydrolysis profiles in Table 1 were analyzed by numerical solution of the nonequilibrium rate equations with the program SCoP. Scheme 5 fitting employed fixed parameter assignments similar to those used previously (see Appendix and ref *3*), except that *a* joined K_S, k_{-P}, and k_2 as a fourth fitted parameter. The ATMA hydrolysis profiles in Table 1 were fitted to eq 1 with fixed parameters $i = 3$ and $g = 0.01$ to obtain the fitted parameters *a*, iK_S, k_{-P}, and $K_M = K_S K_1$ (see Experimental Procedures). The value of k_2 was calculated as the product of the predetermined k_{cat}/K_{app} and fitted K_M. Values of k_{cat}/K_{app} employed in the analyses were taken from Table 1.

constant *b* in Scheme 5 is allowed to vary, the fitted curves showing both substrate activation and substrate inhibition with W86F AChE (Figure 2C) or wild-type AChE at pH 5.5 (Figure 3A) can be reproduced precisely. The fitted parameters with *a* as a variable are listed in Table 2. In addition to *a*, these parameters include the equilibrium constant K_S for substrate binding to the P-site and the rate constants k_2 and k_{-P}. Table 1 indicates that fitted values of *a* and a_{sa} followed similar trends in the two-site and three-site models, although the *a* values in the two-site model were somewhat larger. Other features of the fitted parameters are considered in the Discussion. The key conclusion here is that the two-site model in Scheme 5 can quantitatively account for triphasic hydrolysis profiles. However, the hydrolysis curves alone when fitted by this two-site model unfortunately did not provide a unique solution. An increase in either *a* or *b* was sufficient to provide a good fit, so these curves do not resolve whether acetylation or deacetylation rate constants are increased during substrate activation.

Substrate Activation Occurs at the Acetylation Step with the Substrate Analogue 3-(Acetamido)-N,N,N-trimethylanilinium (ATMA). If acetylation rates are accelerated during substrate activation, the activating ligand must bind to *E*S, the enzyme intermediate that undergoes acetylation. To test this possibility, substrates for which acetylation is rate-limiting ($k_2 \ll k_3$) are attractive, because they generate very low levels of acetylated enzyme intermediates and allow simplification of Scheme 5. These substrates can be identified because they have low values of the turnover number k_{cat} relative to those for good substrates such as acetylthiocholine, phenyl acetate, and *o*-nitrophenyl acetate. Most low turnover substrates that have been reported, however, such as indophenyl acetate (*36*) and *o*-nitroacetanilide (*37*), are uncharged and thus unlikely to bind to the P-site to give substrate activation. The only low turnover cationic substrate known is the amide analogue of acetylcholine (*38*), for which no convenient spectrophotometric assay is available. Acetanilides are attractive low turnover substrates because acetanilide bonds are much stronger than ester bonds and the formation of aniline products can be monitored by spectrophotometry. Quinn and colleagues have shown that k_{cat}/K_{app} for *o*-nitroacetanilide with AChE is 1000-fold lower than that for *o*-nitrophenyl acetate (*39*) and that k_{cat} values of anilides in general are 1−3 orders of magnitude lower than those of the corresponding aryl esters (*37*). Therefore, we synthesized the acetanilide substrate analogue ATMA, a compound previously examined only as an inhibitor of AChE (*27*, *40*). The structure of this compound is very similar to those of high-affinity A-site ligands such as TMTFA and edrophonium (Figure 1).

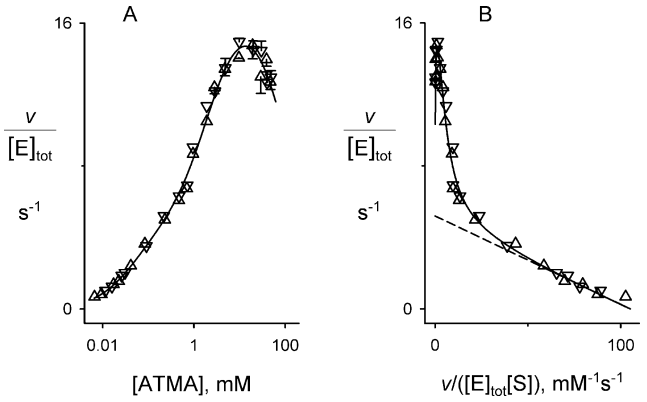

FIGURE 4: Substrate inhibition and activation are apparent during ATMA hydrolysis by human wild-type AChE. Panel A: Plots of $v/[E]_{tot}$ vs [S] for two independent data sets at pH 7.0 (△, ▽). $[E]_{tot}$ corresponded to 35−38 nM. Points at ATMA concentrations above 2 mM are the means of two to four measurements. The solid line was fitted with eq 5 to obtain parameters included in the averages in Table 1. Panel B: Data and fitted lines in panel A were transformed to the Eadie−Hofstee format to clarify the substrate activation phase as in Figure 2.

Hydrolysis of ATMA can be conveniently followed by the absorbance difference with its aniline product at 290 nm. Rates *v* were obtained at initial ATMA concentrations as low as 10 μM, allowing a determination of k_{cat}/K_{app} with wild-type AChE of 105 mM^{-1} s^{-1} (Table 1). This value is about 700-fold lower than that for acetylthiocholine in Table 1, consistent with the previous reports of the relative activity of acetanilides with AChE. The hydrolysis profile in Figure 4A indicated slight substrate inhibition at the highest ATMA concentrations, and the Eadie−Hofstee transformation in Figure 4B revealed significant substrate activation as well. Fitting of the data to eq 5 for the three-site equilibrium model in Scheme 4 gave a substrate activation parameter $a_{sa} = 4.1$ and $K_d = 45$ μM (Table 1). Since k_{cat}/K_{app} is equivalent to k_2/K_d in this model, a k_2 for ATMA of 5 s^{-1} was calculated as the product of k_{cat}/K_{app} and K_d. This estimate of k_2 is about 2000-fold lower than estimates of k_2 and k_3 for acetylthiocholine with wild-type AChE (see Table 2). Since both substrates generate the same acetyl enzyme intermediate and thus are characterized by the same k_3 value, the low k_2 value indicates that acetylation is rate limiting for ATMA ($k_{cat} = k_2$) and that the acetylated enzyme intermediates included in Scheme 5 are negligible. Scheme 5 is then simplified to Scheme 1. Furthermore, the slow acetylation step allows ATMA to equilibrate fully at the A-site, a simplification that allows the steady-state rate equations for Scheme 1 to be solved in a tractable algebraic form (eq 1) without resorting to the numerical integration necessary for Scheme 5.

Equation 1 contains seven variable parameters for fitting of data like that in Figure 4A, and these are reduced to six by independent determination of k_{cat}/K_{app} at low ATMA concentrations. Two of these parameters ($i = 3$ and $g = 0.01$) were fixed, and the remaining four (a, iK_S, k_{-P}, and K_M) were fitted to give the values for the two-site model in Table 2. iK_S is a measure of ATMA affinity for the P-site when ATMA is bound to the A-site (ESS_P in Scheme 1). This affinity ($iK_S = 2.7$ mM) was more than 50-fold lower than the ATMA affinity for the A-site ($K_M = 47$ μM). The fitting was not sensitive to the value of i (fitted parameters varied less than 20% over the range $1 \leq i \leq 10$) because the binary complex ES_P was a very minor species. A value of $i = 3$ was selected on the basis of comparisons with other P-site ligands as noted in Table 5 below. Sensitivity to g also was low (variation less than 20% over the range $0 \leq g \leq 0.04$) except for k_{-P}, which varied nearly 2-fold over this range. The equilibrium assumptions in Scheme 1 and eq 1 were verified by fitting with the same fixed parameters in the nonequilibrium SCoP model (see footnote 7 in the Appendix). Agreement for the four fitted parameters in Table 2 was within 0.3%. Since eqs 5 and 1 reflect equilibrium versions of Schemes 4 and 1, respectively, it is not surprising that the lines fitted to both equations for the data in Figure 4 superimposed precisely and that very similar values of a ($=a_{sa}$), iK_S ($=K_{sa}$), K_M ($=K_d$), and k_2 were obtained from the two schemes (Tables 1 and 2). This agreement emphasizes that both models postulate that substrate activation arises from equilibrium substrate binding to a site distinct from the catalytic or A-site with consequent acceleration of the acetylation reaction k_2. They differ in that Scheme 4 attributes substrate inhibition to substrate binding to a hypothetical third site while Scheme 1 stipulates that both substrate activation and inhibition derive from substrate binding to the P-site with differing effects on acetylation ($a > 1$) and product dissociation ($g \ll 1$).

Confirmation of ATMA Affinities for the A-Site and P-Site in AChE by Titrations with Thioflavin T, a Fluorescent Reporter Ligand. Fitting of kinetic data alone to a mechanistic model like that in Scheme 1 is not sufficient to establish the validity of the model. To gain additional evidence to support Scheme 1, we obtained estimates of K_M and iK_S independent of the kinetic parameters from ATMA hydrolysis. First, we examined ATMA as an inhibitor of acetylthiocholine hydrolysis at low acetylthiocholine concentrations to confirm the prediction that K_I for ATMA as an inhibitor is equal to its K_M in Scheme 1. ATMA behaved as a pure competitive inhibitor, having no effect on the intercepts of reciprocal plots of v^{-1} vs [acetylthiocholine]$^{-1}$ at ATMA concentrations as high as 500 μM (data not shown). Analysis of the reciprocal plot slopes with eq 2 showed a linear dependence on ATMA concentration with a competitive inhibition constant K_I of 30 ± 2 μM. Similar procedures were used to analyze ATMA inhibition of the AChE-catalyzed hydrolysis of *o*-nitrophenyl acetate, and a K_I of 42 ± 3 μM was obtained (data not shown). These K_I determinations are in reasonable agreement with the K_M of 47 ± 6 μM for ATMA from Scheme 1 in Table 2.

A more critical test of Scheme 1 is to assess whether the iK_S for substrate activation determined by fitting the ATMA hydrolysis data to eq 1 agrees with the affinity of ATMA for the P-site. This affinity can be measured independently of kinetic data with fluorescence assays that monitor the equilibrium binding of thioflavin T, a fluorescent ligand that binds specifically to the P-site (*2*). The extension of Scheme 1 that specifically considers interaction of both ATMA and thioflavin T with AChE is given as Scheme 6 in the Appendix. Since it is reasonable to assume that the levels of intermediates involving bound product P are negligible in the fluorescence titrations, Scheme 6 can be simplified to Scheme 2, allowing the titration data to be analyzed with eq 4.[6] The analysis required that the affinity of thioflavin T for the P-site be known (Table 3). AChE was then titrated with varying concentrations of ATMA in the presence of a fixed concentration of thioflavin T as shown in Figure 5A. The initial high fluorescence of the binary complex of thioflavin T and AChE decreased on addition of ATMA. Partial fluorescence quenching was expected at lower ATMA concentrations that bind to the A-site, and a complete loss of fluorescence was anticipated at higher ATMA concentrations as ATMA competed with and displaced thioflavin T from the P-site. Fitting of the data to eq 4 clearly indicated two binding sites for ATMA and supported these expectations. The higher affinity site gave an average equilibrium dissociation constant K_M of 44 ± 3 μM in four independent titrations (Table 4), consistent with binding to the A-site as measured by the K_M value for ATMA in Tables 1 and 2 and the K_I values from hydrolysis inhibition noted above. The fluorescence of thioflavin T in the ternary complex with AChE and ATMA was quenched by a factor of about 3 ($f_{EL}/f_{ELS} = 3.0$; Figure 5A). A similar quenching was reported previously for thioflavin T in the ternary complex with AChE and edrophonium [$f_{EL}/f_{ELI} = 2.8$ (*2*)]. The lower affinity ATMA site gave an average fitted equilibrium dissociation constant iK_S of 4.1 ± 1.0 mM for ATMA binding to the P-site (Table 4). This value is in reasonable agreement with the iK_S value of 2.7 ± 0.4 mM determined from ATMA hydrolysis profiles (Tables 1 and 2), providing strong support for the P-site as the site of substrate activation as proposed in Schemes 1 and 2.

While the agreement in these iK_S values for ATMA binding to the P-site is reassuring, the assignment of iK_S from the fluorescence titration in Figure 5A was less robust than

Table 3: K_L Determinations for Thioflavin T at the P-Site[a]

A-site ligand	kinetic assay (μM)	fluorescence titration (μM)
none	na[b]	1.88 ± 0.20 (1)[c]
none	na	1.89 ± 0.13 (1)[d]
none	1.83 ± 0.10 (1)[e]	na
none	1.3 ± 1.0 (1)[f]	na
echothiophate	na	4.5 ± 0.4 (1)[c]
TMTFA	na	1.11 ± 0.07 (1)[c]

[a] The equilibrium dissociation constant K_L was determined as indicated in the following footnotes and the Experimental Procedures. [b] na, not applicable [c] From fluorescence titration with eq 3 (varying $[E]_{tot}$). [d] From fluorescence titration with eq 3 (varying $[L]_{tot}$). [e] As K_I in eq 2 from the data in Figure 6D. [f] As K_I in eq 2 from the data in Figure 6B. Where indicated, the A-site was occupied by irreversible diethylphosphorylation with echothiophate or slowly reversible binding of TMTFA (see Experimental Procedures).

[6] Testing this assumption by fitting the data in Figure 5A to the full Scheme 6 with the SCoP program resulted in changes of less than 3% in the four fitted parameters when intermediates involving bound P were included.

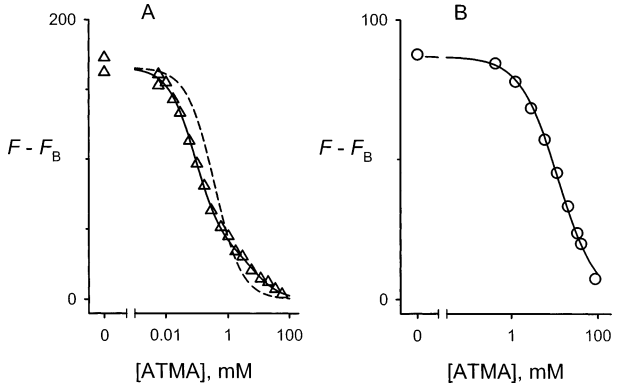

FIGURE 5: The ATMA affinity for the P-site of wild-type AChE determined with thioflavin T as a fluorescent reporter agrees with that calculated from ATMA hydrolysis profiles. The fluorescence of thioflavin T bound to the P-site at the indicated ATMA concentrations was measured for 60 s at an emission wavelength of 490 nm as outlined in the Experimental Procedures. The dependence of F on the ATMA concentration was then fitted to eq 4. The fluorescence F_B without AChE was measured in parallel, and points and the fitted lines are plotted as $F - F_B$. Panel A: Samples contained thioflavin T (6 μM) and unmodified AChE (290 nM). After temperature equilibration for 20 s, a slight linear increase in fluorescence with time (due in part to hydrolysis of ATMA) was corrected by extrapolation to the initial fluorescence (F) at the time of mixing. Equation 4 was fitted with K_L fixed at the predetermined value of 1.83 μM (Table 3) and i and i_2 set at 3 to give $K_M = 46 \pm 5$ μM, $iK_S = 3.8 \pm 0.5$ mM, $f_{EL} = 890 \pm 20$ nM^{-1}, and $f_{EL}/f_{ELS} = 3.0 \pm 0.2$ (solid line). These K_M and iK_S values are included in the averages in Table 2. The maximal value of F_B was 7.3 at the highest ATMA concentration. The dashed line corresponds to the fit when the data are forced to a single site version of eq 4 (f_{EL} fixed at 890 nM^{-1} and K_M^{-1} fixed at 0). Panel B: The A-site of AChE (240 nM) was blocked by pretreatment with echothiophate, and thioflavin T was adjusted to 7 μM. Equation 4 was fitted to a single site with K_L fixed at the predetermined value of 4.5 μM (Table 3), i set at 1, and K_M^{-1} set at zero to give $iK_S = 4.6 \pm 0.3$ mM and $f_{EL} = 590 \pm 20$ nM^{-1}. This iK_S value is included in the average in Table 4. The maximal value of F_B was 27.9. The cuvette size differed in panels A and B, so f_{EL} and F_B values in these panels are not comparable.

Table 4: iK_S and K_M Determinations for ATMA at the A- and P-Sites[a]

	iK_S		K_M	
A-site ligand	kinetic assay (mM)	fluorescence titration (mM)	kinetic assay (μM)	fluorescence titration (μM)
none	2.7 ± 0.4 (6)[b]	4.1 ± 1.0 (4)[c]	47 ± 6 (6)[b]	44 ± 2 (4)[c]
ECHO[d]	na[e]	5.2 ± 0.5 (11)[f]	na	na
TMTFA	na	0.70 ± 0.03 (7)[g]	na	na

[a] Equilibrium dissociation constants iK_S and K_M were determined as indicated in the following footnotes and the Experimental Procedures. [b] From the kinetic assays in Table 2. [c] From fluorescence titration with eq 4 (as in Figure 5A). [d] Echothiophate. [e] na, not applicable. [f] From fluorescence titration with eq 4 (as in Figure 5B). [g] From fluorescence titration with eq 4 [varying [ATMA] with K_L for thioflavin T fixed at the predetermined value of 1.11 ± 0.07 μM (Table 3) and i assigned as 1].

its evaluation from the hydrolysis profiles in Figure 4. For example, the fitting was more sensitive to the fixed values of i and i_2 imposed in eq 4. Over the range $1 \leq i = i_2 \leq 10$, the fitted values of K_M and iK_S varied by as much as a factor of 2 from the values determined with $i = i_2 = 3$ in Figure 5A and Table 2. Two steps were taken to minimize this concern. First, an i_2 of 3 was measured independently in Figure 6A below. Fixing i_2 at 3 eliminated virtually all of the variation in fitted values of K_M and iK_S over the range $1 \leq i \leq 10$. Second, the fluorescence titration was repeated after blocking the A-site. In this case ATMA can only compete directly with thioflavin T for binding to the P-site. Two blocking agents specific for the A-site were used. Echothiophate is an organophosphate that blocks the A-site by forming a covalent diethoxyphosphorylated adduct with S203 in the A-site. Titration of this modified AChE with ATMA in the presence of thioflavin T gave profiles consistent with a single ATMA binding site with an equilibrium dissociation constant iK_S of 5.2 ± 0.5 mM (Figure 5B and Table 4). Diethylphosphorylation of S203 does alter the affinity of ligands for the P-site, as the K_L for thioflavin T increased from 1.8 to 1.9 μM before echothiophate treatment to 4.5 μM after treatment (Table 3). Thus, iK_S for ATMA binding to the P-site of this modified AChE is expected to correspond closely to iK_S for ATMA binding to the P-site in the unmodified enzyme, and this is the observed result. A second A-site-specific blocking agent employed was TMTFA (Figure 1), a transition state analogue that forms a tetrahedral adduct with S203 (*12*). Titration of TMTFA-modified AChE with ATMA in the presence of thioflavin T also gave profiles consistent with a single ATMA binding site (data not shown), but here the fitted equilibrium dissociation constant iK_S was 0.70 ± 0.03 mM (Table 4). This value is 6-fold lower than the measured iK_S with unmodified AChE, indicating that the affinities of ATMA and TMTFA in this ternary complex are slightly higher than the affinity of either ligand in the binary AChE complexes. Since TMTFA is a transition state analogue, this observation indicates that ATMA binding to the P-site stabilizes the transition state for ATMA acetylation at the A-site and explains the observed substrate activation.

Other P-Site Ligands Activate Acetylation Less Effectively than ATMA. Having established that ATMA activates its own acetylation by forming ternary complexes with ATMA bound to both the A- and P-sites, we investigated the effects of two other P-site ligands on substrate hydrolysis in general and relative acetylation rates in particular. The data for one ligand, thioflavin T, complemented the fluorescence data in Figure 5. Thioflavin T inhibited the hydrolysis of both ATMA and acetylthiocholine, but the inhibition was much more pronounced with acetylthiocholine (Figure 6). A similar difference was noted previously for inhibition of the hydrolysis of arylacylamides and acetylthiocholine by the P-site ligands propidium and gallamine (*41*). This difference is expected from the steric blockade feature in our kinetic models. Bound P-site ligands inhibit the hydrolysis of good substrates such as acetylthiocholine primarily by slowing their entry to the A-site. The slower hydrolysis rates of poor substrates such as ATMA are unaffected by their rate of entry since these substrates equilibrate with the A-site before acetylation (*17*, *25*). These differences were quantified by analysis of second-order hydrolysis rate constants z measured at low substrate concentrations with eq 2. The reciprocals of these rate constants increased nearly linearly with thioflavin T concentration for acetylthiocholine hydrolysis (Figure 6D), allowing determination of a K_I for thioflavin T of 1.83 μM with considerable accuracy. The slight curvature in the plot gave the value $\alpha = 0.03$, and this is a good measure of the factor g_2 by which substrate association and product

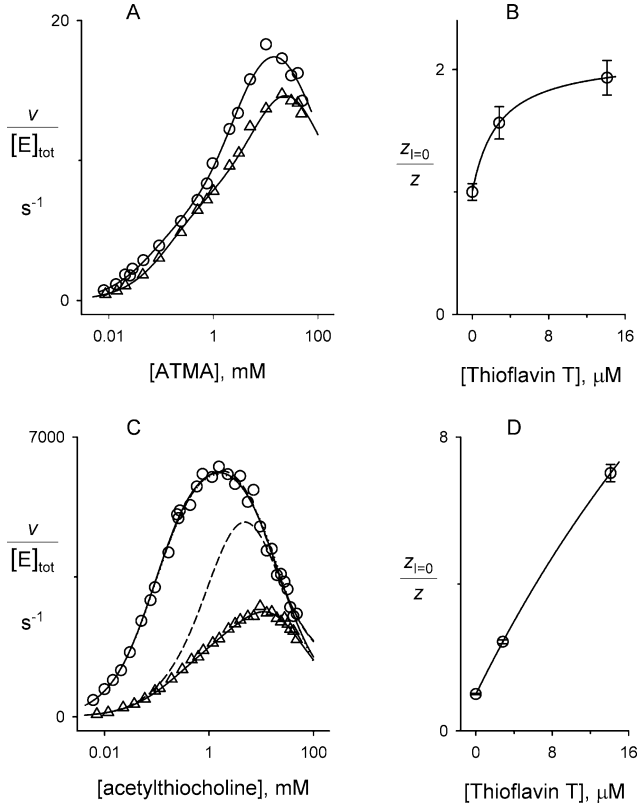

FIGURE 6: Thioflavin T binding to the P-site of AChE inhibits the hydrolysis of ATMA and acetylthiocholine to different extents. Panels A and C: Plots of $v/[E]_{tot}$ vs [S] were generated for ATMA (A) and acetylthiocholine (C) in the presence (△) and absence (○) of 14 μM thioflavin T (I) at pH 7.0. Panel A: The points in the absence of I were first fitted to eq 1 as in Table 1 with k_{-P} fixed at the average value of 700 s^{-1} and a, iK_S, and K_M as the variables (solid line). These parameters as well as $K_I = 1.83$ μM (Table 2) and $g_2 = 0.01$ were then fixed in eq 6, and the points in the presence of I were fitted with a_2 and i_2 as the variables to give $a_2 = 1.42 \pm 0.03$ and $i_2 = 3.14 \pm 0.10$ (solid line). These values are included in the averages for thioflavin T in Table 5. $[E]_{tot}$ corresponded to 34.2 nM. Panel B: Points at low ATMA concentrations in panel A (<240 μM with [I] = 14 μM; <100 μM with [I] = 0 or 3 μM; the 3 μM set is not shown in panel A) were analyzed in reciprocal plots of v^{-1} vs $[S]^{-1}$ as outlined in the Experimental Procedures. The ratios of the slopes of these plots ($z_{I=0}/z$) were fitted as shown to eq 2 to give $K_I = 1.3 \pm 1.0$ μM and $\alpha = 0.47 \pm 0.06$. Panel C: The points in the absence of I were first fitted to the nonequilibrium model in Scheme 5 as in Table 1, with i fixed at 3, k_{-P} fixed at an average value of 1.3×10^5 s^{-1}, and a, K_S, and k_2 as the variables (dotted line largely obscured by upper solid line). The fitting with this model was extended to points in the presence of I in three ways. (1) The previously fitted parameters and all others were fixed, with $a_2 = 1.3$ and $i_2 = 3$ (as determined for ATMA in Table 3 and panel A) and $K_I = 1.83$ μM (Table 3) to give the dashed line. (2) Only a_2 and i_2 were allowed to vary, resulting in a fit of $a_2 = 0.24$ and $i_2 = 0.18$ that nearly superimposed with the lower solid line. (3) Parameters were set as in (1) except c was set to 0, and five parameters (a, K_S, k_2, d, and i_2) were fitted simultaneously to three data sets (the two shown plus a third set at 3 μM thioflavin T) (solid lines). The fitted values of the first three parameters were within 40% of their values in Table 1; $d = 0.32$ and $i_2 = 1.2$. $[E]_{tot}$ corresponded to 100 pM. Panel D: Points at low acetylthiocholine concentrations in panel C (<310 μM with [I] = 14 or 3 μM; <170 μM with [I] = 0) were analyzed in reciprocal plots of v^{-1} vs $[S]^{-1}$ as in panel B. The ratios of the slopes of these plots ($z_{I=0}/z$) were fitted as shown to eq 2 to give $K_I = 1.83 \pm 0.10$ μM and $\alpha = 0.031 \pm 0.010$.

dissociation are slowed by the bound thioflavin T (*6*, *17*). In contrast, the second-order rate constants for ATMA varied by only a factor of 2 over the entire range of thioflavin T concentrations (Figure 6B), and the pronounced curvature in the plot lowered the precision of the K_I estimate. The value $\alpha = 0.47$ is consistent with an absence of steric blockade and provides a check of other kinetic constants as noted below.

Table 5: Effects of P-Site Ligands on ATMA Hydrolysis[a]

P-site ligand	K_I (μM)	a_2	i_2
thioflavin T	1.83 ± 0.10 (1)	1.3 ± 0.1 (2)	3.1 ± 0.1 (2)
propidium	1.55 ± 0.13 (1)	0.8 ± 0.3 (4)	9.5 ± 1.9 (4)

[a] ATMA hydrolysis rates were measured in the presence and absence of the indicated P-site ligand, and the data were fitted first to eq 1 and then to eq 6 as described in Figure 6A. The indicated K_I for each ligand was measured independently with acetylthiocholine as in Figure 6D and fixed in the eq 6 analysis with a_2 and i_2 as the only variables.

The fact that ATMA equilibrates with the A-site before acetylation allows explicit solution of its rate equation (eq 6) from Scheme 6 (in the Appendix) over the entire range of ATMA and thioflavin T concentrations. Analysis of the data with this equation was carried out in two steps in Figure 6A, first by fitting kinetic parameters to the data in the absence of thioflavin T and then fixing these parameters to fit the two remaining variables a_2 and i_2 introduced by the addition of thioflavin T (Table 5). The i_2 value of 3.1 ± 0.1 is a measure of the extent to which thioflavin T and ATMA affinities decrease in their ESI_P ternary complex with AChE relative to their affinities in the binary complexes. This i_2 value is slightly smaller than corresponding i_2 estimates of 5−7 for ternary complexes with propidium at the P-site (*17*). If i_2 values reflect slight unfavorable electrostatic interactions between the two cationic ligands in a ternary complex, one would expect a larger i_2 with propidium because it has two positive charges (this is also observed in Table 5). The a_2 value of 1.3 ± 0.1 indicates that thioflavin T slightly accelerates ATMA acetylation in the ESI_P ternary complex but not to the extent measured in the ESS_P complex when ATMA is bound to the P-site. Comparison of eqs 2 and 6 reveals that α in eq 2 should be equivalent to a_2/i_2 in eq 6, and the calculated a_2/i_2 of 0.43 was in good agreement with the α of 0.47. An analysis similar to that in Figure 6A,B was conducted with propidium as the P-site ligand (data not shown). The value of a_2 with propidium was about 1 (Table 5), further indicating that P-site ligands vary in their ability to accelerate the acetylation of substrates at the A-site. However, these data continue to support our previous contention that, with the exception of the neurotoxin fasciculin, P-site ligands do not induce an allosteric modulation in the A-site that inhibits the acetylation rate constant (i.e., a_2 values do not fall below 1).

Deacetylation Appears To Be Delayed until Product Dissociates from the EAP Complex. We returned to the analysis of hydrolysis over the entire range of acetylthiocholine concentrations with Scheme 5 and investigated whether kinetic constants measured with ATMA could be applied to this substrate. The ATMA data clearly show that substrate activation does involve the acetylation step, thus justifying the assignment of $a > 1$ rather than $b > 1$ in the two-site model for acetylthiocholine in Table 2. The analyses with ATMA also indicate that i is likely to be greater than 1 for acetylthiocholine. This change had a very minor effect on the fitting of the data sets in Table 1. After repeating these fits with $i = 3$, a increased by 50%, but iK_S, k_{-P}, and

k_2 were altered by less than 6%. More interesting results were obtained when Scheme 5 was extended as outlined in the Appendix to allow analysis over the entire range of acetylthiocholine concentrations in the presence of a P-site ligand like thioflavin T. Three fitting procedures were applied (Figure 6C). In the first, fixed values of $a_2 = 1.3$ and $i_2 = 3$ obtained from the ATMA analyses were simply imposed on the best fit parameters obtained in the absence of thioflavin T. This procedure gave the dashed line in Figure 6C and clearly failed to provide sufficient inhibition by thioflavin T at higher acetylthiocholine concentrations near the maximum in v. More inhibition could be obtained in a second procedure that fitted a_2 and i_2 to values of less than 0.25 (Figure 6C). While this fit superimposed reasonably well with the data, these values, particularly that of i_2, are not reasonable. The i_2 value indicates ligand affinities in the ESI$_P$, EAPI$_P$, and EPI$_P$ ternary complex that are more than 5-fold higher than the respective affinities in the binary complexes. Such an increase is inconsistent with the i_2 values in Table 5 and has not been measured for closely related ternary complexes (except for those involving the transition state analogue TMTFA, as noted in the preceding section). More inhibition also could be obtained in a third fitting procedure that suggests a new feature of the AChE catalytic mechanism. Rather than increase the level of inhibition by simply forcing the inhibitor to bind more tightly in the ESI$_P$, EAPI$_P$, and EPI$_P$ intermediates on the catalytic pathway, the inhibition could be increased by raising the relative level of at least one of the ES, EAP, and EP intermediates to which the inhibitor can bind. This could be achieved by imposing a decrease in the product dissociation rate constant k_{-P}, but such a decrease results in an unreasonable k_{-P} value (see Discussion). Instead, we set the value of c in Scheme 5 to zero. This assignment means that deacetylation cannot occur in EAP and EAPI$_P$ until the product dissociates. Since the bound P-site ligand slows the product dissociation rate, the $c = 0$ assignment increased the relative level of EAPI$_P$ by nearly an order of magnitude. Setting c to zero had only a small effect on data fitting in the absence of a P-site ligand. After the fits of the data sets in Table 2 were repeated with $c = 0$ and $i = 3$, a and iK_S increased by about factors of 2 while k_{-P} and k_2 changed by less than 30% from the tabulated values. However, when three data sets over a range of thioflavin T concentrations were analyzed simultaneously with five variable parameters, good fits were obtained (solid lines in Figure 6C) with a fitted i_2 value of 1.2. Therefore, the observed level of thioflavin T inhibition was consistent with an i_2 value greater than 1 if c was set to zero.

DISCUSSION

The mechanistic basis of substrate activation and substrate inhibition with cholinesterases in general has been unresolved, especially when triphasic substrate hydrolysis profiles that show both phenomena are observed. As outlined in the Results, it is a special challenge to account for both phenomena simultaneously with a model that includes only the A- and P-sites of AChE. A two-site model with only three intermediates was proposed to account for triphasic acetylthiocholine substrate activation and inhibition curves with *Drosophila* AChE (*42*). While this model is very concise, the kinetic constants derived from the fitting of substrate hydrolysis data do not appear realistic. For example, the fitted substrate affinity for the P-site decreased by a factor of 10^4 when substrate bound to the A-site, a difference that is not supported by independent data. In a later report, this research group shifted to a three-site model similar to that in Scheme 4 and attributed substrate inhibition to a decrease in the deacylation rate constant when substrate bound to the inhibition site (*34*). The kinetic constants obtained for their triphasic acetylthiocholine hydrolysis profile with *Drosophila* AChE in fact resemble those determined for human AChE with our three-site model in Table 1. Their estimate that substrate occupancy of the inhibition site would slow deacetylation by a factor of 25 was particularly noteworthy. The validity of this estimate was tested by measuring the effects of several cationic ligands that bind to the AChE A- and/or P-sites on decarbamoylation, a deacylation rate constant that can be isolated from other steps in the catalytic pathway. Carbamic acid esters form intermediate carbamoyl enzymes analogous to the acetyl enzyme in Scheme 5, but carbamoyl enzymes are hydrolyzed with a deacylation rate constant k_3 that is some 10^7 times smaller than k_3 for the acetyl enzyme. Most of the cationic ligands, including a ketone analogue of acetylcholine, increased the apparent k_3 for decarbamoylation by factors of 2−7, and none decreased k_3 by more than 40% (*34*). These observations appear to rule out the hypothesis that substrate inhibition involves a blockade of deacylation.

Substrate activation has been less evident with wild-type mammalian and electric organ AChEs than with insect AChE and BChE, but the similar three-dimensional structures of these enzymes (*43*, *44*) strongly argue that they do not have fundamentally different catalytic mechanisms. Substrate activation is seen with acetylthiocholine and mammalian AChE mutants, including F297I (*45*) and W86F (Figure 2), with a cationic carbamate substrate and eel AChE (*46*), and to a small extent with acetylthiocholine and wild-type AChE between pH 5 and pH 7 (*35*; Figure 3 and Table 1). One advantage of the introduction of ATMA as an AChE substrate is that it clearly reveals substrate activation with wild-type human AChE. Furthermore, the fact that the acetylation rate constant k_2 is so much slower for ATMA than for acetylthiocholine allowed us to demonstrate that substrate activation involves the acetylation step and to simplify the kinetic mechanism in an equilibrium model. Substrate activation is less evident with acetylthiocholine and wild-type AChE because acetylation in this case is only partially rate-limiting, and acceleration of the acetylation step has only a modest effect on the overall hydrolysis rate. However, fitting of these hydrolysis profiles to Scheme 5 with $i = 3$ and $c = 0$ results in a value of a that approaches 3−4, indicating that the increase in the acetylation rate constant with acetylthiocholine bound at the P-site is similar to that with ATMA even though the resulting substrate activation is cryptic.

It is worthwhile to place this work in the context of our recent efforts to characterize the complete catalytic pathway in AChE by returning to our proposed model with the 10 enzyme species in Scheme 5. To allow analysis of this model, we have minimized the number of rate constants that involve these species with one simple principle: Assume that reaction rate constants at either the A- or P-site remain unaltered by additional ligand occupancy unless there is experimental evidence to the contrary. If there were no such evidence,

this assumption would eliminate all but seven rate constants in Scheme 5 (because all of the lettered coefficients *a*, *b*, *c*, *d*, *g*, and *i* would equal 1), and all AChE substrates would follow simple Michealis−Menten kinetics. However, the following evidence is to the contrary. First, many cationic substrates show substrate inhibition at high concentrations. This is accommodated in Scheme 5 by setting $g \ll 1$, our steric blockade proposal. Steric blockade accounted not only for substrate inhibition (*3*, *6*) but also for the kinetics of ligand binding in AChE ternary complexes (*17*) and for the extent of inhibition of substrate hydrolysis by P-site ligands (*6*, *25*; Figure 6). Second, a few cationic substrates show substrate activation at intermediate concentrations. This phenomenon was readily apparent for ATMA, and analysis of Schemes 1 and 6 indicated that it arises from $a > 1$. Third, the slight inhibition of ATMA hydrolysis by P-site ligands indicated that $i_2 > 1$ (Table 5) and, by analogy, that $i > 1$. Finally, application of the finding that $i_2 > 1$ to the inhibition of acetylthiocholine hydrolysis by P-site ligands suggested a new feature of the catalytic mechanism, namely, that *c* in Scheme 5 approaches zero (Figure 6C). We return to this suggestion in the Discussion below.

Our analysis of ATMA hydrolysis not only showed that substrate activation resulted from acceleration of the acetylation step in the catalytic pathway but also allowed one test of the proposal in Scheme 1 that the site responsible for substrate activation is the P-site. The affinity of ATMA for the substrate activation site as measured from the substrate hydrolysis profile was compared to the affinity of ATMA for the P-site determined by fluorescence titration, and the two values of iK_S were in agreement (Table 4). Therefore, conformational interaction between the A- and P-sites to promote enzyme acylation is triggered when both are bound with this cationic substrate. The detailed enzyme conformational movements that mediate this interaction remain to be clarified. It may seem paradoxical that, in Scheme 1, substrate binding to a single P-site can give rise to both substrate activation and substrate inhibition. However, these effects are linked to different steps in the catalytic pathway. The extent of substrate activation is essentially proportional to the substrate occupancy of the P-site. In contrast, substrate inhibition lags far behind substrate occupancy of the P-site, because it only becomes detectable when the product dissociation rate is slowed sufficiently from a relatively high initial value to become rate-limiting. Quantitative final confirmation of the model in Scheme 1 would be obtained if the value of $k_{-P} = 700\ s^{-1}$ obtained for the 3-amino-*N*,*N*,*N*-trimethylanilinium product generated during the hydrolysis of ATMA (Table 2) agreed with an independent direct measurement of k_{-P} as a ligand dissociation rate constant. This rate constant has not yet been measured by rapid kinetic techniques, but it can be estimated as the product of the equilibrium dissociation constant K_P and the association rate constant k_P. Numerous studies with AChE have shown good correspondence between the equilibrium dissociation constant (as measured, e.g., by fluorescence titration) and the inhibition constant K_I for ligands that bind to the catalytic site (e.g., refs *2*, *7*, and *47* and Tables 3 and 4). The K_I for 3-amino-*N*,*N*,*N*-trimethylanilinium was determined to be $70 \pm 10\ \mu M$ (data not shown). Association rate constants for the binding of monoquaternary cationic ligands to mammalian AChE range from 1.3×10^8 to $9 \times 10^8\ M^{-1}\ s^{-1}$ (*4*). When the product of these constants is calculated, it initially appears to disagree with the k_{-P} obtained from the ATMA hydrolysis profile. Even at the low end of the association rate constant range, the product of the rate constant and K_I is $9000\ s^{-1}$, more than an order of magnitude larger than the k_{-P} value in Table 2. While this discrepancy might appear to create a problem for the application of Scheme 1 to the hydrolysis of ATMA, it in fact provides independent evidence in support of the following new proposal that $c \cong 0$ in Scheme 5.

The new feature of the AChE catalytic pathway that we propose involves the initial intermediate formed by acetylation of S203. In this *E*AP intermediate, the alcohol leaving group (e.g., thiocholine when the substrate is acetylthiocholine) has not yet dissociated from the A-site. In Scheme 5, this intermediate can either deacetylate with rate constant ck_3 or undergo product dissociation with rate constant dk_{-P}. Deacetylation involves hydrolysis of the acetic acid ester bond in *E*AP, and three-dimensional structures suggest that a water molecule assumes the location of the cleaved leaving group in order to attack the carbonyl carbon. Therefore, it is quite reasonable to propose that deacetylation is slowed until the leaving group dissociates (i.e., $c \cong 0$). The initial evidence we have presented to support this proposal was drawn from the fitting of the hydrolysis curves for acetylthiocholine in the presence of thioflavin T (Figure 6C) to Scheme 5. After restricting i_2 and k_{-P} to reasonable values, best fits to the data in Figure 6C were obtained by allowing *c* to approach zero. Additional evidence was provided by the value of k_{-P} fitted from the ATMA hydrolysis data (Table 2). As noted in the preceding paragraph, the fitted k_{-P} of $700\ s^{-1}$ is an order of magnitude smaller than the value predicted from k_PK_P. Other kinetic constants determined by fitting the ATMA hydrolysis data to eqs 1 and 6, including iK_S, K_M, and i_2, as noted above, are consistent with independent ligand binding measurements, providing strong support for the model in Schemes 1 and 6. These schemes are easily adapted to the assignment of $c \cong 0$. As the value of ck_3 in Scheme 5 falls below that of dk_{-P}, the intermediate that gives rise to substrate inhibition in Scheme 1 becomes *E*AP rather than *E*P. This slight revision of Scheme 1 is outlined in Scheme 3. In this scheme the formats of Scheme 1 (and Scheme 6) remain the same, but *E*P, EPS_P, and EPI_P are replaced by *E*AP, $EAPS_P$, and $EAPI_P$, respectively; and k_{-P} (in Scheme 3 and eqs 1 and 6) is redefined as dk_{-P}. In other words, all determinations of ATMA kinetic parameters in Tables 1 and 3 remain valid except that now $dk_{-P} = 700\ s^{-1}$. If k_{-P} were $9000\ s^{-1}$ as suggested above, then *d* would correspond to 0.08.

Scheme 3

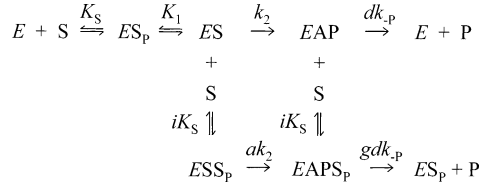

Further evidence in support of the proposal that $c \cong 0$ is provided by recent striking observations on the interaction of rivastigmine with AChE by Bar-On et al. (*48*). Rivastigmine, a potent inhibitor of AChE, is currently in use for the

treatment of Alzheimer's disease under the trade name of Exelon. It is an ester of *N*,*N*-methylethylcarbamic acid, and its potent inhibition arises in part from the fact that it forms a carbamoyl enzyme like those noted earlier in the Discussion. The carbamoyl AChEs generated by the reaction of *N*,*N*-methylethylcarbamoyl chloride with AChEs from various species exhibited typical hydrolysis rate constants k_3 ranging from 0.02 to 0.2 min^{-1} (*48*), and the rivastigmine leaving group NAP [3-[1-(dimethylamino)ethyl]phenol] itself was a rapidly reversible inhibitor of AChE with an affinity ($K_I = 0.5\ \mu M$) comparable to that of other cationic phenols (*48*). However, the rate of hydrolytic reactivation of rivastigmine-inhibited AChE was only 10^{-4} min^{-1} (*48*), more than 2 orders of magnitude slower than expected from the k_3 for decarbamoylation. The slow reactivation was not due simply to stabilization of the carbamoylated enzyme by NAP, as addition of NAP during reactivation of AChE carbamoylated with *N*,*N*-methylethylcarbamoyl chloride had no effect on the observed k_3. Analysis of the three-dimensional crystal structure of rivastigmine-inhibited *Torpedo* AChE suggested an explanation for the slow reactivation, as both the carbamoyl group and NAP remained in the A-site but were detached from each other (*48*). This complex would correspond to *E*AP, where A is the carbamoyl group, in Scheme 3. Furthermore, in the crystal structure the catalytic histidine that participates in decarbamoylation was rotated out of its normal catalytic triad position, indicating a structural reason for *c* to approach zero and dramatically slow the hydrolytic reactivation rate constant ck_3.

The AChE-rivastigmine crystal structure suggests the more general concept that the *E*AP complex produced from the substrate by acylation differs from that generated when added product binds to preformed *E*A. The orientation of the NAP leaving group in the A-site of this structure differed from that in a crystal structure of NAP with AChE alone (*48*), and incubation of carbamoylated enzyme with NAP had no effect on the observed k_3. The extent of the structural difference between *E*APs formed by these two routes may become more pronounced as the substrate structure varies from that of the physiological substrate acetylcholine, and the factor *d* in the dk_{-P} rate constant for product dissociation from *E*AP produced from substrate may be a very sensitive measure of this difference. For example, *d* for NAP dissociation from *E*AP produced from rivastigmine would have to be smaller even than *c* (<0.01) to result in such dramatic stabilization of this *E*AP. Thus NAP and the carbamoyl group mutually interfere with the other's release from the enzyme. On the other hand, the expected k_{-P} for thiocholine calculated as $k_P K_P$ (1.3×10^5 s^{-1}; *6*) agreed with the k_{-P} value fixed in Figure 6C, and the fitted *d* of 0.32 indicated relatively little interference with thiocholine release from the acetyl enzyme intermediate. The *d* of 0.08 calculated above for the *E*AP produced by ATMA falls between these two extremes.

APPENDIX

Three-Site Model of Substrate Hydrolysis. A simple model to account for both substrate inhibition and substrate activation over a full range of substrate concentrations is presented in Scheme 4. This model assumes that the enzyme *E* contains three sites that bind substrate S: the active site where hydrolysis occurs (with substrate dissociation constant K_d

Scheme 4

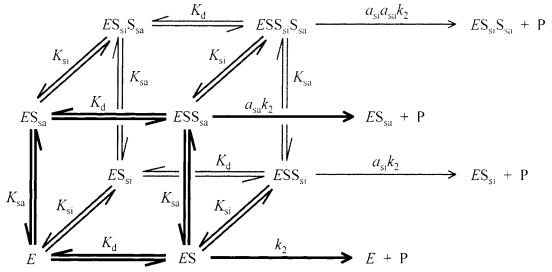

and turnover rate constant k_2); and two nonproductive sites, a substrate inhibition site (with dissociation constant K_{si}) and a substrate activation site (with dissociation constant K_{sa}) (*49*). Binding at each of the three sites is assumed to be independent (i.e., affinities are unaffected by substrate occupancy of other sites) and to reach equilibrium. However, binding of substrate to the inhibition site decreases substrate turnover ($a_{si} < 1$) while binding of substrate to the activation site increases substrate turnover ($a_{sa} > 1$). The rate equation obtained from Scheme 4 (normalized by the total enzyme concentration $[E]_{tot}$) is given in eq 5.

$$\frac{v}{[E]_{tot}} = \frac{\frac{k_2}{K_d}[S]\left(1 + \frac{a_{sa}[S]}{K_{sa}}\right)\left(1 + \frac{a_{si}[S]}{K_{si}}\right)}{\left(1 + \frac{[S]}{K_d}\right)\left(1 + \frac{[S]}{K_{sa}}\right)\left(1 + \frac{[S]}{K_{si}}\right)} \qquad (5)$$

This equation may be considered as an extension of the Haldane equation for substrate inhibition (*3*, *32*). When K_{sa}^{-1} and a_{si} are set to zero, it essentially reduces to the Haldane equation. After fixing k_2/K_d ($\equiv k_{cat}/K_{app}$) at the value measured at low substrate concentration (as outlined in the preceding section) and setting a_{si} to zero, data were fitted to eq 5 by weighted nonlinear regression analysis with Fig.P (BioSoft, version 6.0; weighting assumed that v has a constant percent error) to obtain fitted values of K_d, K_{si}, K_{sa}, and a_{sa}. Conversion of the data to the Eadie−Hofstee format [corresponding to $v/[E]_{tot}$ vs $v/([E]_{tot}[S])$; *50*, *51*] allowed substrate activation to be displayed graphically as a deviation of points above the theoretical line without activation. This line was calculated (i.e., *y*-intercept $= k_2$ and slope $= -K_d$) from the k_2/K_d value measured at low substrate concentration and the K_d value determined from eq 5.

Scheme 5

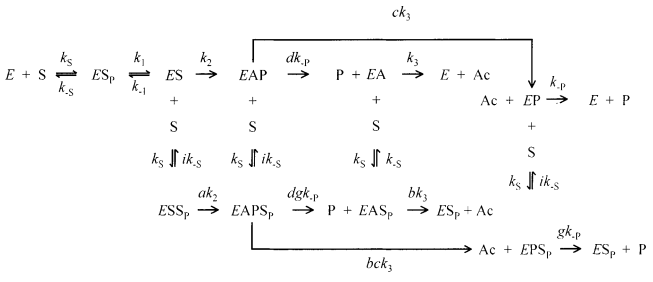

Two-Site Model of Substrate Hydrolysis. Scheme 5 is a two-site model of substrate hydrolysis with AChE from which we recently introduced the concept of steric blockade (*3*, *6*). In this scheme, *E*S represents an ester substrate S bound to the A-site, *E*A is an intermediate in which the enzyme is acetylated, and P is the alcohol leaving group of

the substrate generated by acetylation of the enzyme. *E*S, *E*AP, *E*A, and *E*P are intermediates involving only the A-site, and S can bind to the P-site (designated by subscript P) in each of these intermediates as well as in the free enzyme *E*. For example, ESS_P represents a ternary complex with one S molecule at the A-site and a second at the P-site, and the acylation rate constant k_2 is altered by the factor a in this ternary complex. In general, the 10 enzyme species specified in this scheme are related by 22 independent rate constants. Scheme 5 reduced the number of independent rate constants to the 13 shown largely by assuming that only 3 rate constants (k_{-S}, k_{-S}, and ik_{-S}) characterized substrate binding to the P-site regardless of ligand occupancy at the A-site. Reversible reactions were not assumed to reach equilibrium. Fitting of the steady-state differential equations corresponding to Scheme 5 with a numerical solver in the program SCoP was conducted as described (*3*). Five of the 13 remaining individual or combined independent rate constants were again fixed by separate measurement or conservative approximations [k_{cat}/K_{app}; g; k_3; $B = k_S K_{app}/k_{cat}$; and $R/R_S = 1 + (1.5 - 1.5B^{1-})/(1 + k_2/k_{-1})$].[7] The value of k_{cat}/K_{app} was measured as a single parameter at low substrate concentrations as noted above, because precise estimates of the individual k_{cat} and K_{app} values inserted previously (*3*) are difficult to obtain when substrate activation is observed. The steric blockade model (*3*) further simplified Scheme 5 by assuming that only one reaction is not independent, product dissociation (i.e., $a = b = c = d = i = 1$, but $g < 1$ because product dissociation is slowed from $EAPS_P$ and EPS_P), thereby reducing the number of fitted variable parameters to three (k_2, k_{-P}, and $K_S = k_{-S}/k_S$). Herein, a value of 0.01 was again assigned to g (*3*, *6*, *17*), but a or b was allowed to vary as a fourth fitted parameter to account for substrate activation.

When thioflavin T was included as an inhibitor I during AChE hydrolysis over the entire range of acetylthiocholine concentrations, Scheme 5 was expanded by including five more intermediates: EI_P, ESI_P, $EAPI_P$, EAI_P, and EPI_P, where the subscript P indicates binding of I to the P-site. The expanded scheme is not shown here explicitly, but the reader should visualize a set of relative rate constants for these intermediates parallel to those involving S_P species in Scheme 5 that are indicated by the subscript 2 (i.e., a_2k_2, b_2k_3, g_2k_{-P}, and i_2k_{-I}). These additional rate constants were incorporated into the nonequilibrium numerical solutions and assigned the values $a_2 = b_2 = i_2 = 1$ except where noted. The parameter g_2 defined the relative rate constant both for product P dissociation from the A-site and for S association with the A-site when the P-site was occupied by I (g_2 corresponds to k_{S2}/k_S and k_{-P2}/k_{-P} in ref *6*). The value of g_2 was fixed at 0.03, as determined by the measured value of α in Figure 6D (*17*).

Extension of the Two-Site Model of ATMA Hydrolysis. The inclusion of a P-site ligand as an inhibitor (I) during AChE-catalyzed ATMA hydrolysis requires the extension of Scheme 1 to Scheme 6.

Scheme 6

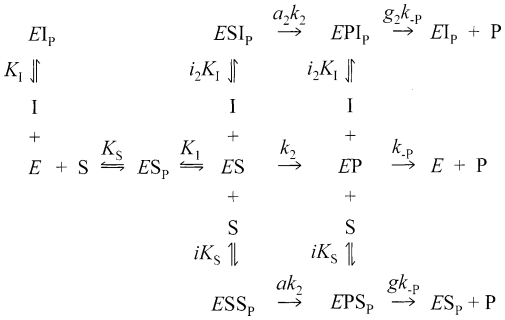

In Scheme 6, the affinities of S and I in the ternary complex ESI_P and of I in EPI_P are decreased by the factor i_2 relative to their affinities in the respective binary complexes; the acylation rate constant k_2 is altered by the factor a_2 in the ESI_P complex; and the dissociation rate constant k_{-P} of the product is altered by the factor g_2 in the EPI_P complex. Other constants were defined in Scheme 1. The steady-state equations for Scheme 6 may be solved algebraically to give eq 6. With the fitting procedure described in Figure 6A and

$$\frac{v}{[E]_{tot}} = \frac{k_2\frac{[S]}{K_M}\left(1+\frac{a[S]}{iK_S}+\frac{a_2[I]}{i_2K_I}\right)}{1+\frac{i[S]}{iK_S}+\frac{[I]}{K_I}+\frac{[S]}{K_M}\left(1+\frac{[S]}{iK_S}+\frac{[I]}{i_2K_I}\right)\left[1+\frac{k_2}{k_{-P}}\frac{\left(1+\frac{a[S]}{iK_S}+\frac{a_2[I]}{i_2K_I}\right)}{\left(1+\frac{g[S]}{iK_S}+\frac{g_2[I]}{i_2K_I}\right)}\right]} \quad (6)$$

Table 5, determinations of a_2 and i_2 were insensitive to the fixed value of g_2. Over the range $0 \le g_2 \le 0.05$, a_2 and i_2 in Table 5 varied by less than 2%.

[7] The approximations and their rationales were as follows: For wild-type AChE, previous assignments of $B = 1.2$ and $k_3 = k_2$ (*3*) were maintained at all pH values, because all four of these rate constants decrease in parallel on protonation of an enzyme group with a pK_a value of 6.1−6.5 (*4*, *5*). The parameter R/R_S was increased from 1.1 at pH 7.0 to 1.2 at pH 5.5 and 1.24 at pH 5.0 because k_{-1} was assumed independent of pH (*4*). For W86F AChE, k_3 was set at the value fitted for the wild-type enzyme, because k_{cat} values determined for acetylthiocholine and phenyl acetate with wild-type enzyme and for phenyl acetate with W86F AChE were identical within error (data not shown) and thus largely limited by k_3. In addition, B was increased to 15 for W86F AChE, on the basis of the observed k_{cat}/K_{app} values and the assumption that k_S was unchanged from that for wild-type AChE, and R/R_S was set to 2.1 because of the increased B value and the calculated decrease in k_2 relative to wild-type AChE. As found previously with wild-type AChE (*3*), varying B and R/R_S over their entire range and g up to 0.04 had little effect (less than a factor of 2) on the fitted parameters for W86F AChE. For ATMA with wild-type AChE, fixed parameters were calculated assuming the same values of k_3, k_S, and k_{-1} as for acetylthiocholine.

REFERENCES

1. Rosenberry, T. L., and Scoggin, D. M. (1984) *J. Biol. Chem. 259*, 5643−5652.
2. De Ferrari, G. V., Mallender, W. D., Inestrosa, N. C., and Rosenberry, T. L. (2001) *J. Biol. Chem. 276*, 23282−23287.
3. Mallender, W. D., Szegletes, T., and Rosenberry, T. L. (2000) *Biochemistry 39*, 7753−7763.
4. Radic, Z., and Taylor, P. (2001) *J. Biol. Chem. 276*, 4622−4633.
5. Rosenberry, T. L. (1975) Acetylcholinesterase, in *Advances in Enzymology* (Meister, A., Ed.) Vol. 43, pp 103−218, John Wiley & Sons, New York.
6. Szegletes, T., Mallender, W. D., Thomas, P. J., and Rosenberry, T. L. (1999) *Biochemistry 38*, 122−133.
7. Taylor, P., and Lappi, S. (1975) *Biochemistry 14*, 1989−1997.
8. Sussman, J. L., Harel, M., Frolow, F., Oefner, C., Goldman, A., Toker, L., and Silman, I. (1991) *Science 253*, 872−879.
9. Karlsson, E., Mbugua, P. M., and Rodriguez-Ithurralde, D. (1984) *J. Physiol. (Paris) 79*, 232−240.
10. Marchot, P., Khelif, A., Ji, Y.-H., Masnuelle, P., and Bourgis, P. E. (1993) *J. Biol. Chem. 268*, 12458−12467.

11. Raves, M. L., Harel, M., Pang, Y.-P., Silman, I., Kozikowski, A. P., and Sussman, J. L. (1997) *Nat. Struct. Biol. 4*, 57−63.
12. Harel, M., Quinn, D. M., Nair, H. K., Silman, I., and Sussman, J. L. (1996) *J. Am. Chem. Soc. 118*, 2340−2346.
13. Tara, S., Elcock, A. H., Kirchhoff, P. D., Briggs, J. M., Radic, Z., Taylor, P., and McCammon, J. A. (1998) *Biopolymers 46*, 465−474.
14. Nachmansohn, D., and Wilson, I. B. (1951) *Adv. Enzymol. 12*, 259−339.
15. Aldridge, W. N., and Reiner, E. (1969) *Biochem. J. 115*, 147−162.
16. Radic, Z., Reiner, E., and Taylor, P. (1991) *Mol. Pharmacol. 39*, 98−104.
17. Szegletes, T., Mallender, W. D., and Rosenberry, T. L. (1998) *Biochemistry 37*, 4206−4216.
18. Changeux, J.-P. (1966) *Mol. Pharmacol. 2*, 369−392.
19. Shi, J., Boyd, A. E., Radic, Z., and Taylor, P. (2001) *J. Biol. Chem. 276*, 42196−42204.
20. Augustinsson, K. B., Bartfai, T., and Mannervik, B. (1974) *Biochem. J. 141*, 825−834.
21. Eriksson, H., and Augustinsson, K. B. (1979) *Biochim. Biophys. Acta 567*, 161−173.
22. Cauet, G., Friboulet, A., and Thomas, D. (1987) *Biochem. Cell Biol. 65*, 529−535.
23. Masson, P., Froment, M.-T., Bartels, C. F., and Lockridge, O. (1996) *Eur. J. Biochem. 235*, 36−48.
24. Marcel, V., Palacios, L., Pertuy, C., Masson, P., and Fournier, D. (1998) *Biochem. J. 329*, 329−334.
25. Mallender, W. D., Szegletes, T., and Rosenberry, T. L. (1999) *J. Biol. Chem. 274*, 8491−8499.
26. Laemmli, U. K. (1970) *Nature 227*, 680−685.
27. Berman, J. D., and Young, M. (1971) *Proc. Natl. Acad. Sci. U.S.A. 68*, 395−398.
28. Ellman, G. L., Courtney, K. D., Andres, J. V., and Featherstone, R. M. (1961) *Biochem. Pharmacol. 7*, 88−95.
29. Riddles, P. W., Blakeley, R. L., and Zerner, B. (1979) *Anal. Biochem. 94*, 75−81.
30. Camps, P., Cusack, B., Mallender, W. D., El Achab, R., Morral, J., Muñoz-Torrero, D., and Rosenberry, T. L. (2000) *Mol. Pharmacol. 57*, 409−417.
31. Lakowicz, J. R. (1999) *Principles of Fluorescence Spectroscopy*, Kluwer Academic/Plenum, New York.
32. Haldane, J. B. S. (1930) *Enzymes*, p 84, Longmans and Green, New York.
33. Masson, P., Xie, W., Froment, M. T., and Lockridge, O. (2001) *Biochim. Biophys. Acta 1544*, 166−176.
34. Brochier, L., Pontie, Y., Willson, M., Estrada-Mondaca, S., Czaplicki, J., Klaebe, A., and Fournier, D. (2001) *J. Biol. Chem. 276*, 18296−18302.
35. Masson, P., Schopfer, L. M., Bartels, C. F., Froment, M. T., Ribes, F., Nachon, F., and Lockridge, O. (2002) *Biochim. Biophys. Acta 1594*, 313−324.
36. Krupka, R. M. (1975) *Biochim. Biophys. Acta 410*, 120−129.
37. Barlow, P. N., Acheson, S. A., Swanson, M. L., and Quinn, D. M. (1987) *J. Am. Chem. Soc. 109*, 253−257.
38. Moore, D. E., and Hess, G. P. (1975) *Biochemistry 14*, 2386−2389.
39. Acheson, S. A., Barlow, P. N., Lee, G. C., Swanson, M. L., and Quinn, D. M. (1987) *J. Am. Chem. Soc. 109*, 246−252.
40. Toomik, R., Eller, M., and Jarv, J. (1988) *Eesti NSV Tead. Akad. Toim., Keem. 37*, 30−36.
41. Costagli, C., and Galli, A. (1998) *Biochem. Pharmacol. 55*, 1733−1737.
42. Stojan, J., Marcel, V., Estrada-Mondaca, S., Klaebe, A., Masson, P., and Fournier, D. (1998) *FEBS Lett. 440*, 85−88.
43. Harel, M., Kryger, G., Rosenberry, T. L., Mallender, W. D., Lewis, T., Fletcher, R. J., Guss, J. M., Silman, I., and Sussman, J. L. (2000) *Protein Sci. 9*, 1063−1072.
44. Nachon, F., Nicolet, Y., Viguie, N., Masson, P., Fontecilla-Camps, J. C., and Lockridge, O. (2002) *Eur. J. Biochem. 269*, 630−637.
45. Radic, Z., Pickering, N. A., Vellom, D. C., Camp, S., and Taylor, P. (1993) *Biochemistry 32*, 12074−12084.
46. Tomlinson, G., Mutus, B., and McLennan, I. (1980) *Mol. Pharmacol. 18*, 33−39.
47. Mooser, G., and Sigman, D. S. (1974) *Biochemistry 13*, 2299−2307.
48. Bar-On, P., Millard, C. B., Harel, M., Dvir, H., Enz, A., Sussman, J. L., and Silman, I. (2002) *Biochemistry 41*, 3555−3564.
49. Clery, C., Bec, N., Balny, C., Mozhaev, V. V., and Masson, P. (1995) *Biochim. Biophys. Acta 1253*, 85−93.
50. Eadie, G. S. (1942) *J. Biol. Chem. 146*, 85−93.
51. Hofstee, B. H. J. (1952) *Science 116*, 329−331.

BI027065U